Originally Published in: Shun Morizumi, Seidai Sato, Kazuya Koyama, Hiroyasu Okazaki, Yajuan Chen, Hisatsugu Goto, Kozo Kagawa, Hirohisa Ogawa, Haruka Nishimura, Hiroshi Kawano, Yuko Toyoda, Hisanori Uehara, Yasuhiko Nishioka. Blockade of Pan-Fibroblast Growth Factor Receptors Mediates Bidirectional Effects in Lung Fibrosis. American Journal of Respiratory Cell and Molecular Biology 2020; Volume 63, Issue 3: Pages 317-326.
DOI: 10.1165/rcmb.2019-0090OC

Blockade of Pan-fibroblast Growth Factor Receptors Mediates Bidirectional Effects in Lung Fibrosis

Shun Morizumi[1], Seidai Sato[1], Kazuya Koyama[1], Hiroyasu Okazaki[1], Yajuan Chen[1], Hisatsugu Goto[1], Kozo Kagawa[1], Hirohisa Ogawa[2], Haruka Nishimura[1], Hiroshi Kawano[1], Yuko Toyoda[1], Hisanori Uehara[3], Yasuhiko Nishioka[1]

[1]Department of Respiratory Medicine and Rheumatology, Graduate School of Biomedical Sciences, Tokushima University, Tokushima, Japan

[2]Department of Pathology and Laboratory Medicine, Graduate School of Biomedical Sciences, Tokushima University, Tokushima, Japan

[3]Division of Pathology, Tokushima University Hospital, Tokushima, Japan

Running title: Dual effects of FGFR inhibition in lung fibrosis

Address correspondence and reprint requests to: Yasuhiko Nishioka, M.D., Ph.D., Department of Respiratory Medicine and Rheumatology, Graduate School of Biomedical Sciences, Tokushima University, 3-18-15 Kuramoto-cho, Tokushima 770-8503, Japan. Phone: +81-88-633-7127; Fax: +81-88-633-2134

E-mail: yasuhiko@tokushima-u.ac.jp

AJRCMB Articles in Press. Published April 27, 2020 as 10.1165/rcmb.2019-0090OC

Author Contributions

Conception and design: S.M., S.S. and Y.N.; Analysis and interpretation: S.M., S.S., K.Koyama., H.O., Y.C., H.G., K.Kagawa., H.O., H.N., H.K., Y.T., H.U., and Y.N.; drafting the manuscript for important intellectual content: S.M., S.S., and Y.N.; all authors have approved the final version and agree to be accountable for all aspects of the work in ensuring that questions related to the accuracy or integrity of any part of the work are appropriately investigated and resolved.

This article has an online data supplement, which is accessible from this issue's table of content online at www.atsjournals.org.

AJRCMB Articles in Press. Published April 27, 2020 as 10.1165/rcmb.2019-0090OC

Abstract

[Rationale] Fibroblast growth factors (FGF) are major factors associated with the pathogenesis of pulmonary fibrosis. Nintedanib, a tyrosine kinase inhibitor targeting several growth factor receptors including the FGF receptor (FGFR), has been approved for the treatment of idiopathic pulmonary fibrosis (IPF). On the other hand, recent reports suggest that FGF are required for epithelial recovery. In this study, we focused on FGF signaling to both fibroblasts and alveolar epithelial cells (AECs), and examined the effect of a pan-FGFR blocker on experimental pulmonary fibrosis in mice.

[Methods] The effects of BGJ398, a pan-FGFR inhibitor, on the migration and proliferation of fibroblasts and AECs were assessed using transwell migration or ^{3}H-thymidine incorporation assays. The expression of FGFR was analyzed using immunoblot or flow cytometry. We also investigated the effect of BGJ398 on the pulmonary fibrosis induced by bleomycin in mice.

[Results] Both lung fibroblasts and AECs expressed FGFRs. BGJ398 significantly inhibited the proliferation and migration of lung fibroblasts stimulated with FGF2. BGJ398 also reduced the proliferation of AECs in response to FGF2. Although the administration of BGJ398 ameliorated pulmonary fibrosis in bleomycin-treated mice, it increased mortality due to alveolar injury and inhibition of AEC regeneration.

[Conclusions] These data suggest that the total inhibition of FGFR signaling can suppress

AJRCMB Articles in Press. Published April 27, 2020 as 10.1165/rcmb.2019-0090OC

lung fibrosis by inhibiting fibroblast activities, although alveolar injury is simultaneously caused.

Key Words: Fibroblast growth factor, pulmonary fibrosis, epithelial recovery

Abbreviations:

IPF idiopathic pulmonary fibrosis

FGF fibroblast growth factor

FGFR FGF receptor

PDGFR platelet-derived growth factor receptor

VEGFR vascular endothelial growth factor receptor

AEC alveolar epithelial cells

BLM bleomycin

^{3}H-TdR [^{3}H] thymidine deoxyribose

FACS fluorescence-activated cell sorter

BAL bronchoalveolar lavage

NS normal saline

AJRCMB Articles in Press. Published April 27, 2020 as 10.1165/rcmb.2019-0090OC

Introduction

Idiopathic pulmonary fibrosis (IPF) is a refractory fibrotic disease characterized by progressive loss of the lung function and median survival of 3-4 years. Characteristic pathological features are the proliferation of fibroblasts and deposition of extracellular matrix (1-3).

Recently, treatment with nintedanib led to reduction in the annual rate of decline of the forced vital capacity in patients with IPF (4). Nintedanib is an inhibitor of receptor tyrosine kinases targeting fibroblast growth factor receptor (FGFR), platelet-derived growth factor receptor (PDGFR), and vascular endothelial growth factor receptor (VEGFR). These tyrosine kinases have been reported to be related to signaling pathways associated with the progression of fibrosis (5).

Focusing on the inhibitory effect on each receptor, we and others previously reported that the inhibition of PDGFR can ameliorate pulmonary fibrosis (6-9). It has been reported that the targeting of VEGFR signaling could attenuate pulmonary fibrosis (10, 11). However, the effects of FGF/FGFR on pulmonary fibrosis still remain controversial.

Fibroblast growth factors (FGF) have 22 ligands in humans, bind to four receptors (FGFR1-4, and its isoform), and have various functions such as developmental processes, wound healing, and angiogenesis (12-14). FGF signaling is important in the lung maturation process, and

AJRCMB Articles in Press. Published April 27, 2020 as 10.1165/rcmb.2019-0090OC

affects epithelial-mesenchymal interaction (15). FGFR expression occurs in fibroblast foci and also in alveolar epithelial cells (AEC) in the human IPF lung (16), thus, FGF signaling may affect various cells depending on the localization and intensity of expression.

FGF/FGFR have been reported to be involved in the pathogenesis of pulmonary fibrosis (12, 15-19). It was shown that blocking the activation of FGFR by S252W mutant soluble ectodomain of FGFR-2 IIIc alleviated pulmonary fibrosis in mice (17). Another report proposed that mesenchymal FGF signaling is required for the development of pulmonary fibrosis, and that therapeutic strategies aimed directly at mesenchymal FGF signaling could be beneficial in the treatment of pulmonary fibrosis (18). On the other hand, it was suggested that FGF1 has preventative and therapeutic effects on pulmonary fibrosis via inhibiting myofibroblast differentiation and enhancing the proliferation and hyperplasia of AEC (19). The overexpression of FGF2 or the administration of recombinant FGF2 were also reported to ameliorate pulmonary fibrosis of the bleomycin-induced mouse model via inhibiting transforming growth factor beta 1 (TGFβ1) – induced stress fiber formation and serum response factor-dependent gene expression (20). Thus, the significance of FGFR signaling in pulmonary fibrosis is bidirectional.

However, it is important to investigate the effects of the total inhibition of FGF/FGFR signaling pathways from a therapeutic perspective, because FGFR inhibitor is considered a

AJRCMB Articles in Press. Published April 27, 2020 as 10.1165/rcmb.2019-0090OC

future candidate for anti-fibrotic agents based on the inhibitory profile of nintedanib. We therefore examined the effect of pan-FGFR blocker BGJ398 on pulmonary fibrosis using an experimental mouse model.

Materials and Methods

Detailed methods are described in the online supplement.

Proliferation assay

Human lung fibroblasts, murine lung fibroblasts, or murine lung epithelial cells were seeded on a 96-well plate, and cultured with various concentration of FGFR inhibitor BGJ398 in the presence of FGF2 (30 ng/ml) for 48 hours. One μCi/well of [^{3}H] thymidine deoxyribose (^{3}H-TdR) was pulsed for the final 24 hours and the incorporation of ^{3}H-TdR was measured using a liquid scintillation counter (7).

Cell migration assay

Human or murine lung fibroblasts were plated to the upper chamber of an 8-μm-pore cell culture insert in the presence or absence of various concentrations of inhibitors. FGF2 was added to the lower chamber. After 24-hour incubation, cells that had migrated to the bottom surface of the filter were stained with Diff-Quick and counted (21).

AJRCMB Articles in Press. Published April 27, 2020 as 10.1165/rcmb.2019-0090OC

Immunoblot analysis

Cell extracts of murine fibroblast cells (B6), AEC lines (LA4, MLE12), and homogenized lung tissues were lysed and used for immunoblotting as previously described (22).

Bleomycin-induced pulmonary fibrosis in mice

Seven to eight-week-old C57BL/6 mice were purchased from Charles River Japan (Yokohama, Japan). Mice received a single intra-tracheal instillation of 3 or 6 mg/kg bleomycin on day 0. BGJ398 was administered each day by gavage until day 21. Lung tissues analyzed on day 21 were used for the Ashcroft score and hydroxyproline assay.

Histopathology

Right lung tissues were harvested, fixed in 10% formalin, and embedded in paraffin. Three-micrometer-thick sections were stained with hematoxylin and eosin (H&E) or azan mallory. In the quantitative analysis, a numeric fibrotic scale was used (Ashcroft score). The mean score was considered to be the fibrotic score.

Bronchoalveolar lavage

Bronchoalveolar lavage (BAL) was performed with saline (1 mL) using a soft cannula (21). After counting the number of cells in the BAL fluid (BALF), cells were stained with Diff-Quick for cell classification.

AJRCMB Articles in Press. Published April 27, 2020 as 10.1165/rcmb.2019-0090OC

Flow cytometric analysis

The minced lungs were digested, and harvested single-cell suspensions were stained with anti-Ep-CAM Ab, anti-FGFR-1 Ab, and anti-FGFR-2 Ab. The stained cells were analyzed by a FACScan flow cytometer as previously described (22).

Endothelial permeability

Evans Blue dye was utilized as a marker of the endothelial barrier function. C57BL/6 mice received an intranasal instillation of 3 mg/kg NaCl or bleomycin on day 0. After seven days, mice were sacrificed and analyzed. At three hours prior to termination, Evans Blue dye was injected via the tail vein, and the extravasation of dye into BALF was quantified by spectrophotometry.

Immunofluorescence staining

Paraffin-embedded lung sections were stained with primary antibodies at 4°C overnight and subsequently stained with fluorescence-conjugated secondary antibodies and 4', 6-diamidino-2-phenylindole at room temperature for 1 hour. Fluorescence images were captured with a confocal laser scanning microscope. Double-positive cells for pro-SPC and Ki-67 were counted in 5 random fields (22).

AJRCMB Articles in Press. Published April 27, 2020 as 10.1165/rcmb.2019-0090OC

Statistical Analysis

Significances of differences were analyzed by one-way ANOVA followed by Tukey's test or Student's *t*-test for unpaired samples. The survival curve was analyzed by log rank test. *P*-values of less than 0.05 were considered significant. Statistical analyses were performed using GraphPad Prism program Ver.5.01 (*GraphPad* Software Inc.)

Results

Expression of FGFR in lung fibroblasts and alveolar epithelial cells

The expression of FGFR on murine lung fibroblasts and AEC was examined by immunoblot analysis and flow-cytometry. On immunoblot, murine fibroblasts expressed FGFR1, 2, and 3, but not FGFR4. On the other hand, two murine AEC lines expressed FGFR2 and 3 but not FGFR1 and 4 (Figure 1A).

On flow-cytometry, the primary murine AECs, which were recognized as Ep-CAM-positive cells, also expressed only FGFR2 but not FGFR1 (Figure 1B).

We also examined the mRNA expression of FGFRs (Figure E1). Although some results differ at the mRNA levels and protein levels, it was considered to be due to the differences of stability in mRNA and protein. Furthermore, our group had also previously reported the FGFR2 expression on MRC-5 cells which are human lung fibroblasts (22). Taken together, these data

AJRCMB Articles in Press. Published April 27, 2020 as 10.1165/rcmb.2019-0090OC

suggest that both lung fibroblasts and AEC expressed FGFRs.

BGJ398 inhibits the proliferation of lung fibroblasts and alveolar epithelial cells induced by FGF2

It is now widely accepted that FGF2 is a growth factor that stimulates the migration and proliferation of fibroblasts (23). In order to examine the direct effect of the inhibition of FGF signaling on fibroblasts and epithelial cells, we stimulated these cells with FGF2 with or without the pan-FGFR inhibitor BGJ398. The proliferation of human lung fibroblasts induced by FGF2 was inhibited by BGJ398 in a dose-dependent manner (Figure 2A). The same trend was observed for murine lung fibroblasts (Figure 2B) and murine lung epithelial cells (Figure 2C).

BGJ398 inhibits the migration of lung fibroblasts induced by FGF2

We assessed the effect of BGJ398 on the migration of lung fibroblasts induced by FGF2. The number of migrated fibroblasts markedly increased when cells were treated with FGF2. BGJ398 inhibited the migration of human lung fibroblasts (Figure 3A, C) and murine lung fibroblasts (Figure 3B, D) mediated by FGF2.

Taken together, these data show that FGFR inhibition can affect not only the proliferation and migration of fibroblasts but also the proliferation of lung epithelial cells.

AJRCMB Articles in Press. Published April 27, 2020 as 10.1165/rcmb.2019-0090OC

Pan-FGFR inhibition attenuates pulmonary fibrosis

To examine how pan-FGFR inhibition works *in vivo*, we induced pulmonary fibrosis in the mouse lung by bleomycin. Mice received a single intra-tracheal instillation of 6 mg/kg of bleomycin on day 0. After the administration of BGJ398 with a concentration of 20 mg/kg by gavage from days 0 to 21, lung tissues were harvested and analyzed. By the continuous administration of BGJ398, the number of fibrotic lesions in the lungs of bleomycin-treated mice was reduced (Figure 4A, Figure E2, E3, E4, E5). Quantitative histological analysis showed that the Ashcroft fibrotic score was significantly lower in mice treated with bleomycin and BGJ398 than in those treated with bleomycin alone (Figure 4B). A hydroxyproline colorimetric assay also showed a reduced collagen content in the lungs of mice treated with BGJ398 (Figure 4C).

Pan-FGFR inhibition increases the mortality of bleomycin-treated mice

The body weight of mice not exposed to bleomycin increased in a time-dependent manner without any significant difference between vehicle and BGJ398-alone groups. The weight of mice in the bleomycin-alone group started to decrease on days 2 to 3. Surprisingly, in the bleomycin plus BGJ398 group, the body weight started to decrease soon after the intratracheal instillation of bleomycin. The rate of reduction was higher than in the bleomycin-alone group (Figure 5A), but the significant difference was found on only day 3. The body weights of both

AJRCMB Articles in Press. Published April 27, 2020 as 10.1165/rcmb.2019-0090OC

groups were then nearly equal after day 3.

Along with the decrease of body weight, the survival rate in the bleomycin plus BGJ398 group also began to decline from an early period, and as a result, the total survival rate was lower than that in the bleomycin-alone group (Figure 5B).

Even if the administration of BGJ398 was started from day 10, the histology and the Ashcroft score of bleomycin-treated mice was reduced, and the mortality was increased like as the full-day administration (Figure E6).

Because the high mortality might introduce survivorship bias, we reduced dose of bleomycin to 3 mg/kg in next experiments. Furthermore, to avoid the potential bias caused by using single lungs, we analyzed bilateral lung samples. In consequence, although the reduced dose of bleomycin decreased the mortality (Figure E7A), Pan-FGFR inhibition attenuated pulmonary fibrosis as the same as shown above (Figure E7B, E7C).

Pan-FGFR inhibition does not affect infiltration of inflammatory cells into the lungs

To examine why BGJ398 increased the mortality of bleomycin-treated mice, we examined the effects on lung inflammation using BALF. BALF was harvested from mice in each group on days 5 and 7. As shown in Figure 6, treatment with BGJ398 reduced the number of neutrophils in BALF on day 5, but no effects on the number and classification of inflammatory cells were observed on day 7. The concentration of protein contained in BALF supernatant was

AJRCMB Articles in Press. Published April 27, 2020 as 10.1165/rcmb.2019-0090OC

increased in bleomycin-treated group, but not changed by BGJ398 (Figure E8). These results suggest that the analysis of BAL cells showed no finding associated with increased mortality due to BGJ398.

Pan-FGFR inhibition suppresses the activity of fibroblasts induced by FGF2

We examined the expression of α-SMA and the amount of cleaved caspase-3 in lung tissue homogenates. The amounts of cleaved caspase-3 were increased in bleomycin plus BGJ398 group compared with bleomycin alone group (Figure E9A, E9C). On the contrary, the expressions of α-SMA were decreased by BGJ398 (Figure E9B, E9D).

Next, in order to examine the response to cytokines and growth factors of fibroblasts as well as the effects of BGJ398 on those, the mRNA expression of *Col1a1* and *Acta2* were examined using a quantitative PCR. The incubation of murine primary fibroblasts with the FGF2 resulted in the upregulation of *Col1a1* and *Acta2*, which was inhibited by BGJ398 (Figure E10A). However, the inhibitory effects of BGJ398 did not work when fibroblasts were stimulated by TGF-β1 (Figure E10B).

Pan-FGFR inhibition suppresses the proliferation of alveolar epithelial cells and increases vascular leak *in vivo*

Finally, to examine the effects of BGJ398 on epithelial injury and recovery, we harvested lung tissue from the bleomycin plus BGJ398 group on day 5 when their body weight peaked.

AJRCMB Articles in Press. Published April 27, 2020 as 10.1165/rcmb.2019-0090OC

Paraffin-embedded lung sections were stained for pro-SPC and Ki-67, proliferation markers (Figure 7A). The immunohistochemical staining revealed that the number of pro-SPC^{+}Ki-67^{+} cells in the bleomycin plus BGJ398 group was significantly lower than in the bleomycin-alone group (Figure 7B, C). Furthermore, we performed the immunofluorescence by γH2AX and pro-SPC. Although the number of pro-SPC positive cells was not different between bleomycin-alone group and BGJ398-treated bleomycin group, the γH2AX expression, which reflects DNA damage leading cells to apoptosis, was increased in pro-SPC positive cells (Figure E11). Taken together, these data suggest that the pan-FGFR inhibition suppressed the proliferation of AECs and increased the apoptosis of AECs *in vivo*.

Finally, we examined pulmonary vascular permeability by comparing the leakage of Evans blue dye to BALF in the murine lung. Evans blue has a high affinity for albumin in the blood and leaks out of blood vessels when the permeability of blood vessels is enhanced. The mice treated with bleomycin 7 days after the daily administration of normal saline (NS) or BGJ398 were injected with an Evans blue solution via the tail vein. Three hours later, BALF was collected and the Evans blue concentration of BALF was measured. The administration of BGJ398 increased the concentration of Evans blue dye in BALF, indicating the increased vascular permeability of bleomycin-induced murine lungs (Figure 7D).

AJRCMB Articles in Press. Published April 27, 2020 as 10.1165/rcmb.2019-0090OC

Discussion

In this study, we examined the role of a pan-FGFR blocker on pulmonary fibrosis using an experimental mouse model. The results from this study suggest that the total inhibition of FGFR signaling ameliorates pulmonary fibrosis, but also increases mortality.

The twenty-two types of FGF identified in humans are signaling molecules with structural similarity. Although the FGF family was named and characterized by its ability to promote the proliferation of fibroblasts (24), it is now recognized that FGF family members affect not only fibroblasts but also multiple types of cells (17-20, 24). However, currently used anti-fibrotic drugs cannot select cells targeted for their signal inhibition. Furthermore, previous reports targeting molecules of FGF/FGFR signaling have shown varying results (17-20).

Currently, for the treatment of pulmonary fibrosis, it is common to use receptor inhibitors such as nintedanib. Such inhibitors target all FGFRs in general. Nevertheless, no previous reports have evaluated the effects of all FGFR inhibition on the pathology of pulmonary fibrosis. This study is the first to address this important clinical question.

Here we demonstrate that murine epithelial cells express FGFR 2 and 3 but not FGFR 1 and 4, and that murine fibroblasts express FGFR 1, 2, and 3, but not FGFR4. These results complement those reported by MacKenzie B et al. who found that human alveolar epithelial type II cells in the normal lung expressed FGFR2, 3, and 4, and that those cells in IPF lungs

AJRCMB Articles in Press. Published April 27, 2020 as 10.1165/rcmb.2019-0090OC

expressed all FGFRs (16). They also observed FGFR1 and FGFR2 in myofibroblasts of fibroblast foci as well as in overlying hyperplastic bronchiolar basal cells (16). These results indicate that total FGFR inhibition affects not only fibroblasts but also AECs.

According to expectation, BGJ398, a pan-FGFR blocker, suppressed not only the proliferation and migration of fibroblasts but also the proliferation of AEC *in vitro*. Furthermore, in the mouse model, the administration of BGJ398 suppressed the proliferation of AEC, and increased the DNA damage of AEC and the vascular permeability of bleomycin-induced murine lungs. From these results, we considered that the increase of mortality is due to alveolar injury and inhibition of AEC regeneration. The main finding of this study is that the use of pan-FGFR inhibitor for pulmonary fibrosis was suggested to be harmful despite its anti-fibrotic effects. However, contrary to expectation, in the examination of whole lung tissue, the addition of BGJ398 did not change the α-SMA expressions by the administration of BGJ398. This might be due to the fact that FGF2 acts as an antagonist of TGF-β through suppression of the transcriptional activity of SRF (25, 26).

Nintedanib, one of two approved anti-fibrotic drugs, also has an inhibitory effect on FGFR 1, 2, and 3 (27). Nintedanib is effective without causing fatal adverse events *in vivo* or clinically. The reason for this might be that the IC_{50} of nintedanib for FGFR is much higher than that of BGJ398. The IC_{50} values of BGJ398 against FGFR were reported to be 0.9, 1.4, 1.0, and 60

AJRCMB Articles in Press. Published April 27, 2020 as 10.1165/rcmb.2019-0090OC

nM for FGFR1, 2, 3, and 4, respectively (28). In a phase I study of BGJ398 in patients with advanced solid tumors, the maximum tolerated dose (MTD) was determined to be 125 mg once daily (29). In this study, the unbound average steady-state BGJ398 concentration on day 28 of cycle 1 was 6.93 nM after a 125-mg once daily dosing (29). This concentration may be sufficient to inhibit FGFR1, 2, and 3.

On the other hand, the inhibitory effect of nintedanib on the phosphorylation of FGFR was observed at approximately 100-1000 nM (22), and the IC_{50} values of nintedanib for each FGFR were reported to be higher than 257 nM (30). The C max (peak plasma concentration of a drug after administration) of nintedanib in IPF patients who were administered 150 mg of nintedanib twice daily was 34.9 ng/mL (31). Since the molecular weight/molar mass of nintedanib is about 539.62 g/mol, the actual serum concentration of nintedanib can be estimated to be around 50 to 100 nM. Therefore, the inhibitory effects of nintedanib on the FGFR signaling may be extremely weak.

By contrast, although we tried to assess the expression of PDGFR in alveolar type 2 cells by FACS, the results obtained showed that type 2 epithelial cells in normal and bleomycin-treated mice did not express PDGFR-α or -β (data not shown). Furthermore, we previously showed that proliferative effects on fibroblasts are stronger with PDGF than with FGF (7). From examining these findings, with respect to anti-fibrotic capacity, we believe that inhibition of

AJRCMB Articles in Press. Published April 27, 2020 as 10.1165/rcmb.2019-0090OC

the receptor for PDGF is safer and more effective than FGFR inhibition. Indeed, the inhibitory effect for PDGFR of nintedanib is more potent than FGFR inhibition (30). This PDGFR inhibition-based effect may be the main reason that nintedanib is successful as a therapeutic agent.

In developing new anti-fibrotic drugs for pulmonary fibrosis, the present studies emphasize the significance of examining not only its positive effect on fibroblasts but also the expression of target receptors on AEC. Hence, although our results indicate that the inhibition of pan-FGFR is not good, it may be possible that the specific inhibition for each FGF/FGFR molecules is effective. Besides, if we can develop drugs that selectively targets cell populations like fibroblasts, these results may be different.

One limitation of our study is specificity of BGJ398 as FGFR inhibitor. BGJ398 has been reported as a potent and selective pan-FGFR inhibitor in many previous reports. However, in the original report about BGJ398, BGJ398 has been reported to have strong activity to FGFR1/2/3/4, but also have very weak activity to VEGFR2, Abl, Fyn, Kit, Lck, Lyn and Yes (32). These other inhibiting effects might affect the results in the present study. Another limitation is that EpCAM is not a perfectly specific marker for alveolar epithelial cells. Therefore, the possibility that other types of cells were mixed cannot be denied.

In summary, although the inhibition of FGFR signaling contributed to the prevention of

AJRCMB Articles in Press. Published April 27, 2020 as 10.1165/rcmb.2019-0090OC

pulmonary fibrosis by suppressing the proliferation and migration of pulmonary fibroblasts, this inhibition also decreased the survival rate by suppressing the recovery of epithelial cells from injury. The present results may offer new insight into the pathogenesis of and therapeutic strategy for pulmonary fibrosis. In pathways which involve various molecules such the FGF/FGFR signaling pathway, it is important that the experimental approach assesses the role of each molecule using genetic techniques like knockdown or overexpression. Besides, to conduct preclinical research from a therapeutic perspective, it is also important that the approach uses a pan-blocker to determine whether it is totally beneficial or harmful.

Acknowledgements

The authors thank Ms. Tomoko Oka for technical assistance. We also thank the members of the Nishioka lab for their technical advice and fruitful discussions. This study was supported by Support Center for Advanced Medical Sciences, Tokushima University Graduate School of Biomedical Sciences.

Grants

This work was supported by the Japan Society for the Promotion of Science (JSPS) KAKENHI (Grant Number JP16H0530910) and a grant to the Ministry of Health, Labour and Welfare, the Study Group on Diffuse Pulmonary Disorders, Scientific Research/Research on Intractable Diseases (Y.N.; Code Number: 0000025921).

AJRCMB Articles in Press. Published April 27, 2020 as 10.1165/rcmb.2019-0090OC

Disclosures

The authors declare that they have no competing interests.

AJRCMB Articles in Press. Published April 27, 2020 as 10.1165/rcmb.2019-0090OC

References

1) du Bois RM, Weycker D, Albera C, Bradford WZ, Costabel U, Kartashov A, King TE Jr, Lancaster L, Noble PW, Sahn SA, Thomeer M, Valeyre D, Wells AU. Forced vital capacity in patients with idiopathic pulmonary fibrosis: test properties and minimal clinically important difference. *Am J Respir Crit Care Med* 2011;184:1382-1389.

2) King TE Jr, Pardo A, Selman M. Idiopathic pulmonary fibrosis. *Lancet* 2011;378:1949-1961.

3) Raghu G, Collard HR, Egan JJ, Martinez FJ, Behr J, Brown KK, Colby TV, Cordier JF, Flaherty KR, Lasky JA, Lynch DA, Ryu JH, Swigris JJ, Wells AU, Ancochea J, Bouros D, Carvalho C, Costabel U, Ebina M, Hansell DM, Johkoh T, Kim DS, King TE Jr, Kondoh Y, Myers J, Müller NL, Nicholson AG, Richeldi L, Selman M, Dudden RF, Griss BS, Protzko SL, Schünemann HJ; ATS/ERS/JRS/ALAT Committee on Idiopathic Pulmonary Fibrosis. An official ATS/ERS/JRS/ALAT statement: idiopathic pulmonary fibrosis: evidence-based guidelines for diagnosis and management. A*m J Respir Crit Care Med* 2011;183:788-824.

4) Richeldi L, du Bois RM, Raghu G, Azuma A, Brown KK, Costabel U, Cottin V, Flaherty KR, Hansell DM, Inoue Y, Kim DS, Kolb M, Nicholson AG, Noble PW, Selman M, Taniguchi H, Brun M, Le Maulf F, Girard M, Stowasser S, Schlenker-Herceg R, Disse B,

AJRCMB Articles in Press. Published April 27, 2020 as 10.1165/rcmb.2019-0090OC

Collard HR; INPULSIS Trial Investigators. Efficacy and Safety of Nintedanib in Idiopathic Pulmonary Fibrosis. *N Engl J Med* 2014;370:2071-2082.

5) Grimminger F, Günther A, Vancheri C. The role of tyrosine kinases in the pathogenesis of idiopathic pulmonary fibrosis. *Eur Respir J.* 2015;45:1426-1433.

6) Abdollahi A, Li M, Ping G, Plathow C, Domhan S, Kiessling F, Lee LB, McMahon G, Grone HJ, Lipson KE, Huber PE. Inhibition of platelet-derived growth factor signaling attenuates pulmonary fibrosis. J Exp Med 2005;201:925-935.

7) Aono Y, Nishioka Y, Inayama M, Ugai M, Kishi J, Uehara H, Izumi K, Sone S. Imatinib as a novel antifibrotic agent in bleomycin-induced pulmonary fibrosis in mice. *Am J Respir Crit Care Med*. 2005;171:1279-1285.

8) Daniels CE, Wilkes MC, Edens M, Kottom TJ, Murphy SJ, Limper AH, Leof EB. Imatinib mesylate inhibits the profibrogenic activity of TGF-beta and prevents bleomycin-mediated lung fibrosis. *J Clin Invest* 2004;114:1308-1316.

9) Nishioka Y, Azuma M, Kishi M, Aono Y. Targeting platelet-derived growth factor as a therapeutic approach in pulmonary fibrosis. *J Med Invest* 2013;60:175-183.

10) Hamada N, Kuwano K, Yamada M, Hagimoto N, Hiasa K, Egashira K, Nakashima N, Maeyama T, Yoshimi M, Nakanishi Y. Anti-vascular endothelial growth factor gene

AJRCMB Articles in Press. Published April 27, 2020 as 10.1165/rcmb.2019-0090OC

therapy attenuates lung injury and fibrosis in mice. *J Immunol* 2005;175:1224-1231.

11) Ou XM, Li WC, Liu DS, Li YP, Wen FQ, Feng YL, Zhang SF, Huang XY, Wang T, Wang K, Wang X, Chen L. VEGFR-2 antagonist SU5416 attenuates bleomycin-induced pulmonary fibrosis in mice. *Int Immunopharmacol* 2009;9:70-79.

12) Ornitz DM, Itoh N. The Fibroblast Growth Factor signaling pathway. *Wiley Interdiscip Rev Dev Biol* 2015;4:215-266.

13) Ornitz DM, Xu J, Colvin JS, McEwen DG, MacArthur CA, Coulier F, Gao G, Goldfarb M. Receptor specificity of the fibroblast growth factor family. *J Biol Chem* 1996;271:15292-15297.

14) Zhang X, Ibrahimi OA, Olsen SK, Umemori H, Mohammadi M, Ornitz DM. Receptor specificity of the fibroblast growth factor family. The complete mammalian FGF family. *J Biol Chem* 2006;281:15694-15700.

15) Joannes A, Brayer S, Besnard V, Marchal-Sommé J, Jaillet M1, Mordant P, Mal H, Borie R, Crestani B, Mailleux AA. FGF9 and FGF18 in idiopathic pulmonary fibrosis promote survival and migration and inhibit myofibroblast differentiation of human lung fibroblasts in vitro. *Am J Physiol Lung Cell Mol Physiol.* 2016;310:L615-L629.

16) MacKenzie B, Korfei M, Henneke I, Sibinska Z, Tian X, Hezel S, Dilai S, Wasnick R,

AJRCMB Articles in Press. Published April 27, 2020 as 10.1165/rcmb.2019-0090OC

Schneider B, Wilhelm J, El Agha E, Klepetko W, Seeger W, Schermuly R, Günther A, Bellusci S. Increased FGF1-FGFRc expression in idiopathic pulmonary fibrosis. *Respir Res* 2015;16:83.

17) Yu ZH, Wang DD, Zhou ZY, He SL, Chen AA, Wang J. Mutant soluble ectodomain of fibroblast growth factor receptor-2 IIIc attenuates bleomycin-induced pulmonary fibrosis in mice. *Biol Pharm Bull* 2012;35:731-736.

18) Guzy RD, Li L, Smith C, Dorry SJ, Koo HY, Chen L, Ornitz DM. Pulmonary fibrosis requires cell-autonomous mesenchymal fibroblast growth factor (FGF) signaling. *J Biol Chem* 2017;292:10364-10378.

19) Shimbori C, Bellaye PS, Xia J, Gauldie J, Ask K, Ramos C, Becerril C, Pardo A, Selman M, Kolb M. Fibroblast growth factor-1 attenuates TGF-β1-induced lung fibrosis. *J Pathol.* 2016;240:197-210.

20) Koo HY, El-Baz LM, House S, Cilvik SN, Dorry SJ, Shoukry NM, Salem ML, Hafez HS, Dulin NO, Ornitz DM, Guzy RD. Fibroblast growth factor 2 decreases bleomycin-induced pulmonary fibrosis and inhibits fibroblast collagen production and myofibroblast differentiation. *J Pathol.* 2018;246:54-66.

21) Aono Y, Kishi M, Yokota Y, Azuma M, Kinoshita K, Takezaki A, Sato S, Kawano H, Kishi J, Goto H, Uehara H, Izumi K, Nishioka Y. Role of platelet-derived growth

AJRCMB Articles in Press. Published April 27, 2020 as 10.1165/rcmb.2019-0090OC

factor/platelet-derived growth factor receptor axis in the trafficking of circulating fibrocytes in pulmonary fibrosis. *Am J Respir Cell Mol Biol* 2014;51:793-801.

22) Sato S, Shinohara S, Hayashi S, Morizumi S, Abe S, Okazaki H, Chen Y, Goto H, Aono Y, Ogawa H, Koyama K, Nishimura H, Kawano H, Toyoda Y, Uehara H, Nishioka Y. Anti-fibrotic efficacy of nintedanib in pulmonary fibrosis via the inhibition of fibrocyte activity. *Respir Res.* 2017;18:172.

23) Hetzel M, Bachem M, Anders D, Trischler G, Faehling M. Different effects of growth factors on proliferation and matrix production of normal and fibrotic human lung fibroblasts. *Lung* 2005;183:225-237.

24) Kim KK, Sisson TH, Horowitz JC. Fibroblast growth factors and pulmonary fibrosis: it's more complex than it sounds. *J Pathol.* 2017;241:6-9.

25) Sato H, Sato M, Kanai H, Uchiyama T, Iso T, Ohyama Y, Sakamoto H, Tamura J, Nagai R, Kurabayashi M. Mitochondrial reactive oxygen species and c-Src play a critical role in hypoxic response in vascular smooth muscle cells. *Cardiovasc Res* 2005: 67: 714-722.

26) Kawai-Kowase K, Sato H, Oyama Y, Kanai H, Sato M, Doi H, Kurabayashi M. Basic fibroblast growth factor antagonizes transforming growth factor-beta1-induced smooth muscle gene expression through extracellular signal-regulated kinase 1/2 signaling pathway activation. *Arterioscler Thromb Vase Biol* 2004; 24: 1384-1390.

AJRCMB Articles in Press. Published April 27, 2020 as 10.1165/rcmb.2019-0090OC

27) Inomata M, Nishioka Y, Azuma A. Nintedanib: evidence for its therapeutic potential in idiopathic pulmonary fibrosis. *Core Evid*. 2015;10:89-98.

28) Guagnano V, Furet P, Spanka C, Bordas V, Le Douget M, Stamm C, Brueggen J, Jensen MR, Schnell C, Schmid H, Wartmann M, Berghausen J, Drueckes P, Zimmerlin A, Bussiere D, Murray J, Graus Porta D. Discovery of 3-(2,6-dichloro-3,5-dimethoxy-phenyl)-1-{6-[4-(4-ethyl-piperazin-1-yl)-phenylamino]-pyrimidin-4-yl}-1-methyl-urea (NVP-BGJ398), a potent and selective inhibitor of the fibroblast growth factor receptor family of receptor tyrosine kinase. *J Med Chem.* 2011;54:7066-7083.

29) Nogova L, Sequist LV, Perez Garcia JM, Andre F, Delord JP, Hidalgo M, Schellens JH, Cassier PA, Camidge DR, Schuler M, Vaishampayan U, Burris H, Tian GG, Campone M, Wainberg ZA, Lim WT, LoRusso P, Shapiro GI, Parker K, Chen X, Choudhury S, Ringeisen F, Graus-Porta D, Porter D, Isaacs R, Buettner R, Wolf J. Evaluation of BGJ398, a Fibroblast Growth Factor Receptor 1-3 Kinase Inhibitor, in Patients With Advanced Solid Tumors Harboring Genetic Alterations in Fibroblast Growth Factor Receptors: Results of a Global Phase I, Dose-Escalation and Dose-Expansion Study. *J Clin Oncol*. 2017;35:157-165.

30) Wollin L, Maillet I, Quesniaux V, Holweg A, Ryffel B. Antifibrotic and anti-inflammatory activity of the tyrosine kinase inhibitor nintedanib in experimental models of lung fibrosis.

AJRCMB Articles in Press. Published April 27, 2020 as 10.1165/rcmb.2019-0090OC

J Pharmacol Exp Ther. 2014;349:209-220.

31) Ogura T, Taniguchi H, Azuma A, Inoue Y, Kondoh Y, Hasegawa Y, Bando M, Abe S, Mochizuki Y, Chida K, Klüglich M, Fujimoto T, Okazaki K, Tadayasu Y, Sakamoto W, Sugiyama Y. Safety and pharmacokinetics of nintedanib and pirfenidone in idiopathic pulmonary fibrosis. *Eur Respir J*. 2015;45:1382-1392.

32) Guagnano V, Furet P, Spanka C, Bordas V, Le Douget M, Stamm C, Brueggen J, Jensen MR, Schnell C, Schmid H, Wartmann M, Berghausen J, Drueckes P, Zimmerlin A, Bussiere D, Murray J, Graus Porta D. Discovery of 3-(2,6-dichloro-3,5-dimethoxy-phenyl)-1-{6-[4-(4-ethyl-piperazin-1-yl)-phenylamino]-pyrimidin-4-yl}-1-methyl-urea (NVP-BGJ398), a potent and selective inhibitor of the fibroblast growth factor receptor family of receptor tyrosine kinase. *J Med Chem.* 2011;54:7066-83.

AJRCMB Articles in Press. Published April 27, 2020 as 10.1165/rcmb.2019-0090OC

Figure legends

Figure 1. Expression of receptors for fibroblast growth factors on murine lung fibroblasts and alveolar epithelial cells. The expression of fibroblast growth factor receptors (FGFR) 1, 2, 3, 4 and pro-SPC was examined in cell extracts of murine primary cultured lung fibroblasts (B6) and alveolar epithelial cell lines (LA4, MLE12) by immunoblot analysis (A). By flowcytometry, the expressions of FGFR1 and 2 were investigated in primary culture of alveolar epithelial cells from murine lungs as Ep-CAM-positive cells (B). The dotted line indicates the data with control antibody, and the solid line is with anti-FGFR1 antibody or anti-FGFR2 antibody. The western blot was performed twice, and flow-cytometry was performed thrice.

Figure 2. BGJ398 inhibits the proliferation of lung fibroblasts and alveolar epithelial cells in response to fibroblast growth factor 2. The proliferation of MRC-5 (A), B6 (B), and LA4 (C) cells cultured with recombinant fibroblast growth factor 2 (FGF2: 30 ng/mL) and various concentrations of BGJ398 for 48 hours was measured using a ^{3}H-thymidine incorporation assay. Data were analyzed by one-way ANOVA and are presented as means ± SDs (n=4, independent experiments each). For all graphs: * $p<0.05$, ** $p<0.01$ versus the value in the group treated with FGF2 alone.

AJRCMB Articles in Press. Published April 27, 2020 as 10.1165/rcmb.2019-0090OC

Figure 3. BGJ398 inhibits the migration of lung fibroblasts induced by fibroblast growth factor 2. MRC-5 (A) or B6 (B) cells were plated with to the upper chamber with medium in the presence or absence of various concentrations of BGJ398. Medium containing recombinant fibroblast growth factor 2 (FGF2: 30 ng/mL) were added to the lower chamber. After 24-hour incubation, fibroblasts that had migrated to the bottom surface of the filter were counted in 5 random fields per section at 100× magnification. Data were analyzed by one-way ANOVA and are presented as means ± SDs (n=3 in each group). Representative photographs of MRC-5 treated with FGF2 plus various concentrations of BGJ398 (C). Representative photographs of B6 treated with FGF2 plus various concentrations of BGJ398 (D). For all graphs: * $p<0.05$, ** $p<0.01$ versus the value in the group treated with FGF2 alone.

Figure 4. Administration of BGJ398 attenuates pulmonary fibrosis in bleomycin-treated pulmonary fibrosis mouse model. C57BL/6 mice received an intra-tracheal instillation of 6 mg/kg NaCl or bleomycin on day 0.

BGJ398 was administered daily by gavage at 20 mg/kg until day 21. Analyses were performed on day 21. A histological examination was performed by staining with hematoxylin and eosin (H.E) and azan mallory (A) (scale bar = 500 μm). The fibrotic changes in the lung were evaluated using a numeric fibrotic score. A histological examination of the right lung was performed using H&E staining (B) (n=7 in each group). Collagen content in the left lung lobe

AJRCMB Articles in Press. Published April 27, 2020 as 10.1165/rcmb.2019-0090OC

was measured using the hydroxyproline colorimetric assay (C) (n=7 in each group). Data were analyzed by one-way ANOVA and are presented as means ± SDs. For all graphs: * $p<0.05$, ** $p<0.01$ versus the value in the group treated with bleomycin only.

Figure 5. Administration of BGJ 398 increases mortality accompanied by acute loss of body weight in early phase. C57BL/6 mice received an intra-bronchial instillation of 6 mg/kg NaCl or bleomycin (BLM) on day 0. BGJ398 was administered daily by gavage at 20 mg/kg until day 21. The change of body weight in each group (A) and a Kaplan-Meier plot showing survival in each group (B) (n=7: NS / Vehicle, n=8: NS / BGJ398, n=17: BLM / Vehicle, n=26: BLM / BGJ398). The results of body weight on each day were analyzed by one-way ANOVA, and the survival curve was analyzed by log rank test. *$p<0.05$ versus the value in the group treated with bleomycin only.

Figure 6. Analysis of bronchoalveolar lavage fluid in mice treated with bleomycin and BGJ398. C57BL/6 mice received an intra-tracheal instillation of 6 mg/kg NaCl or bleomycin on day 0. BGJ398 was administered daily by gavage at 20 mg/kg until day 5 or 7. The number of cells and percentage of the cell component in BALF on day 5 or 7 were compared (Day5: n=4 in each group, Day7: n=3: NS / Vehicle, n=3: NS / BGJ398, n=5: BLM / Vehicle, n=5: BLM / BGJ398). Data were analyzed by one-way ANOVA and are presented as means ± SDs. *p<0.05 versus the value in the group treated with bleomycin only.

AJRCMB Articles in Press. Published April 27, 2020 as 10.1165/rcmb.2019-0090OC

Figure 7 Administration of BGJ398 inhibits the proliferation of alveolar epithelial cells in bleomycin-induced pulmonary fibrosis in mice. C57BL/6 mice received an intra-tracheal instillation of 6 mg/kg NaCl or bleomycin on day 0. BGJ398 was administered daily by gavage at 20 mg/kg until day 5. The lung tissue in each group was harvested and analyzed on day 5. (A) Paraffin-embedded lung sections were stained with anti-pro-SPC antibody (*green*) and anti-Ki-67 (*red*). Representative images of immunofluorescence staining at a high magnification in bleomycin-treated lungs are shown to confirm the double-positive cells. (B) Representative images of immunofluorescence staining in each group are shown. Arrows indicate double-positive cells for pro-SPC and Ki-67 (scale bar = 50 μm). (C) pro-SPC^{+}Ki-67^{+} cells, defined as proliferating type II alveolar epithelial cells, were counted in 5 random fields per section at x200 magnification using lung sections. The results are shown as the ratio of Ki-67 positive cells in the total pro-SPC positive cells. Data were analyzed by one-way ANOVA and are presented as means ± SDs. For all graphs: * p<0.05, ** p<0.01 versus the value in the group treated with bleomycin only. (D) C57BL/6 mice received an intra-tracheal instillation of 3 mg/kg NaCl or bleomycin on day 0. Seven days later, mice were injected with an Evans blue solution via the tail vein 3 hours before being killed, and BALF was collected. The Evans blue concentration, which reflects the vascular permeability, was measured with absorbance at 620 nm (n=4 in each group). The results were normalized with NS/Vehicle group, and shown as

AJRCMB Articles in Press. Published April 27, 2020 as 10.1165/rcmb.2019-0090OC

fold change. Data were analyzed by one-way ANOVA and are presented as means ± SDs. For all graphs: * $p<0.05$, ** $p<0.01$ versus the value in the group treated with bleomycin only.

AJRCMB Articles in Press. Published April 27, 2020 as 10.1165/rcmb.2019-0090OC

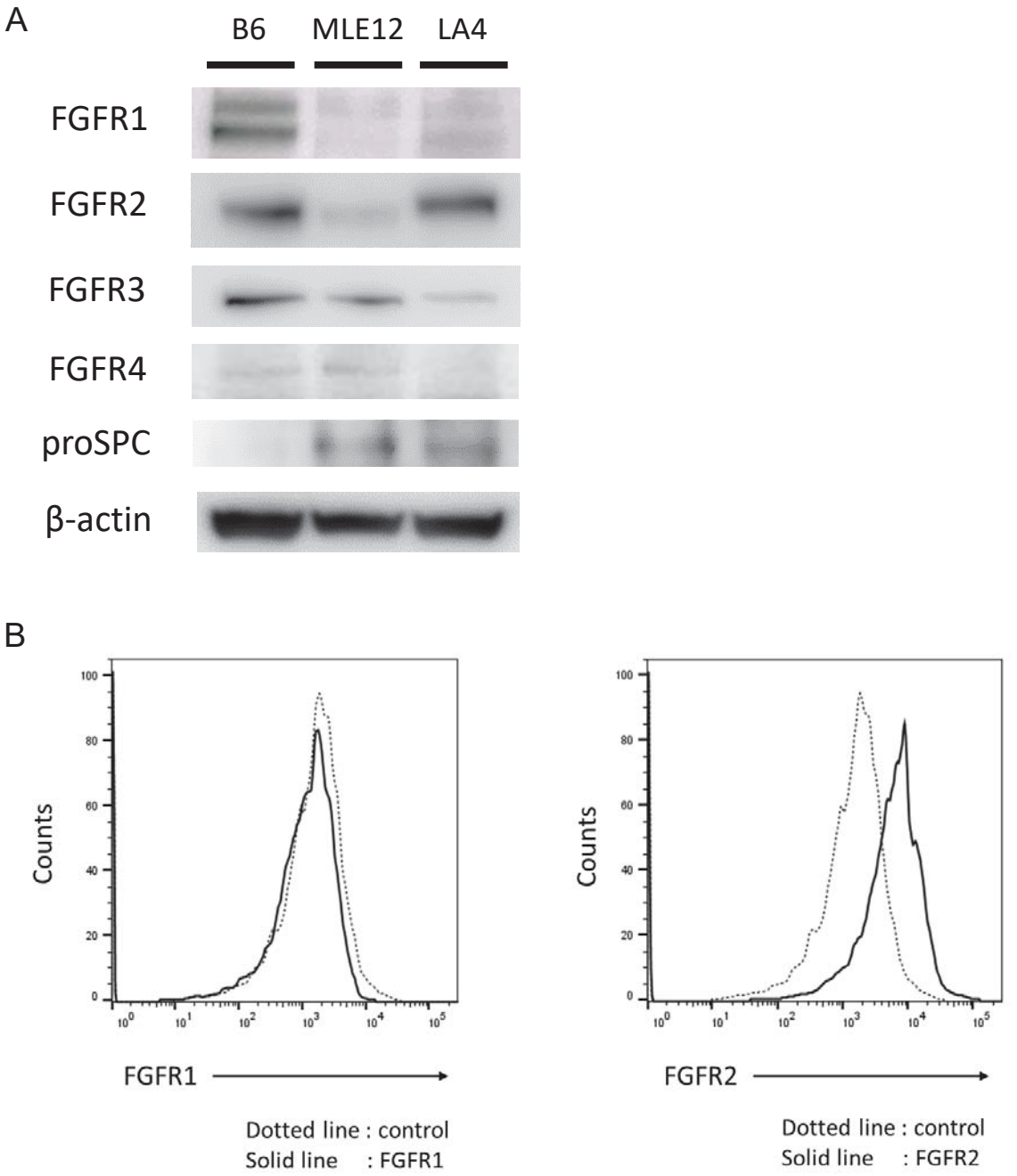

Figure 1

AJRCMB Articles in Press. Published April 27, 2020 as 10.1165/rcmb.2019-0090OC

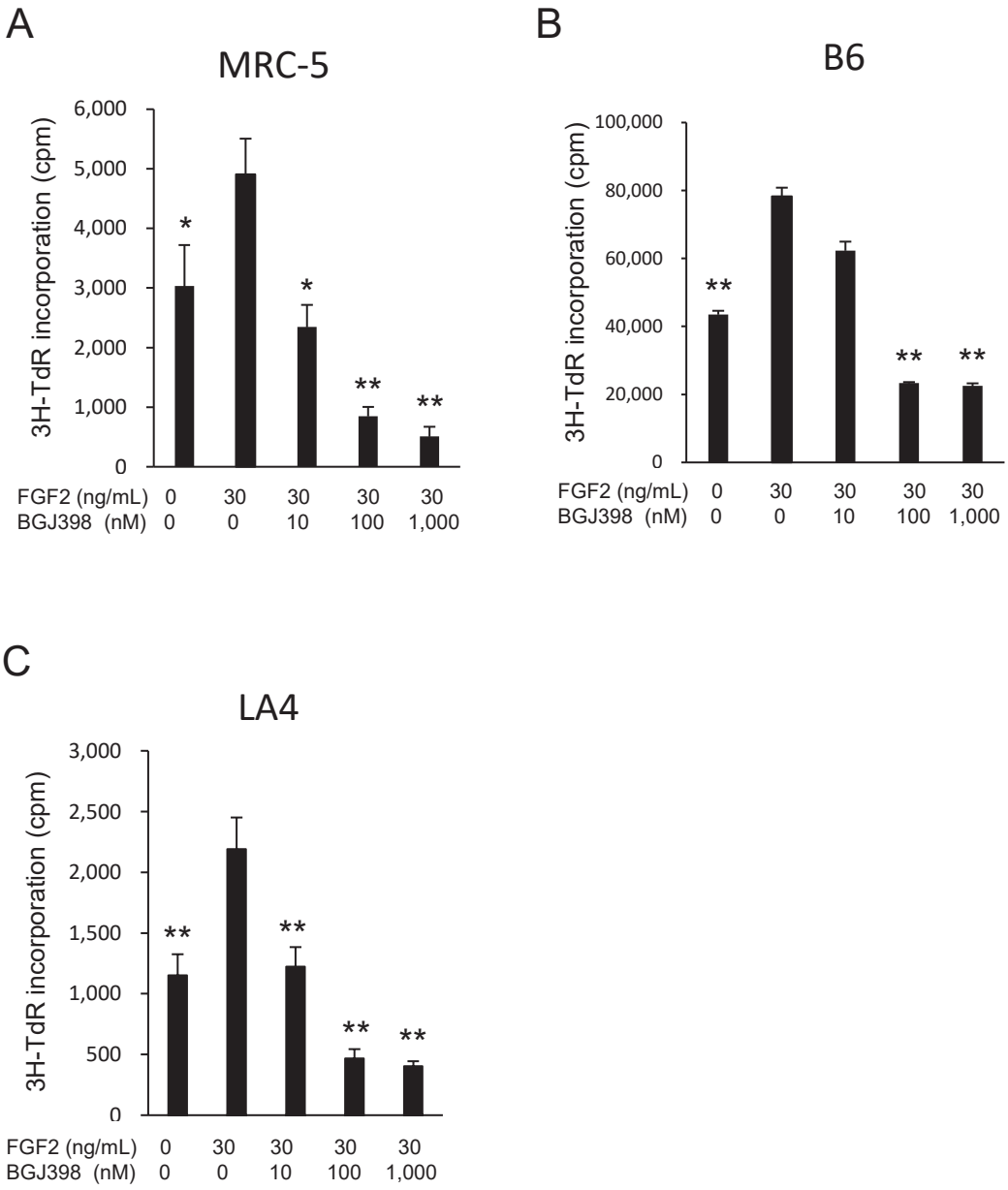

Figure 2

AJRCMB Articles in Press. Published April 27, 2020 as 10.1165/rcmb.2019-0090OC

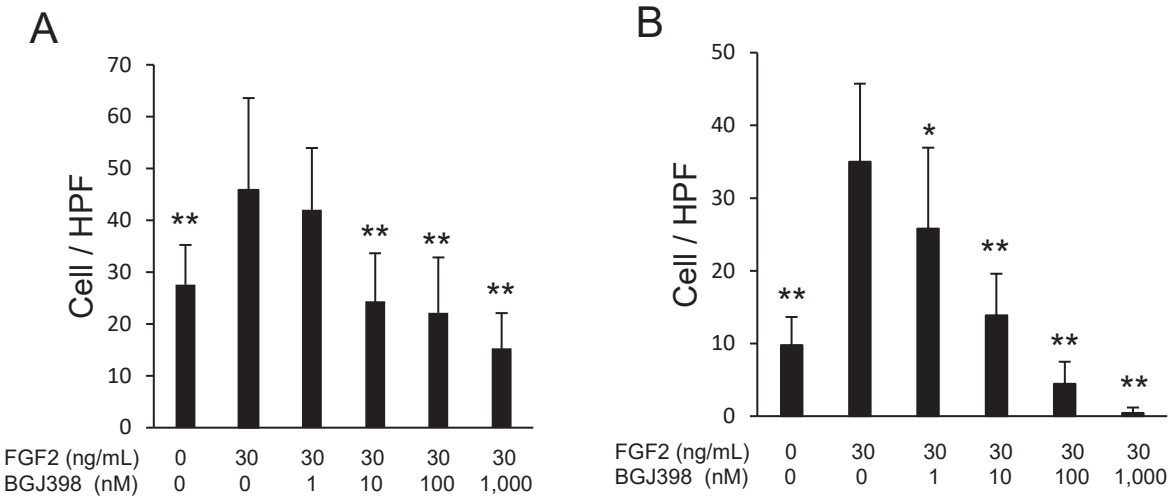

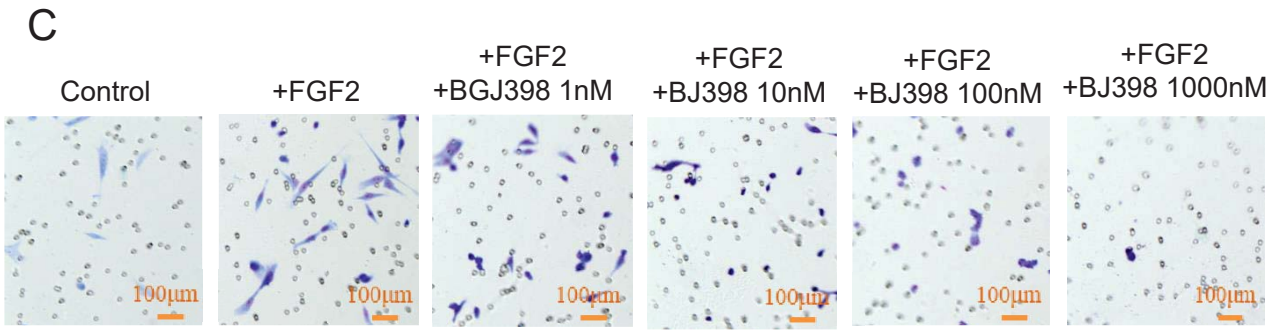

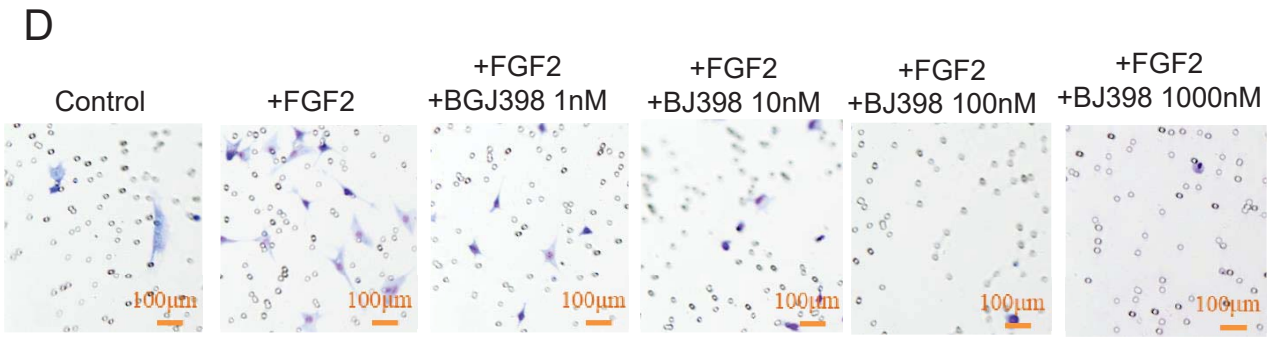

Figure 3

AJRCMB Articles in Press. Published April 27, 2020 as 10.1165/rcmb.2019-0090OC

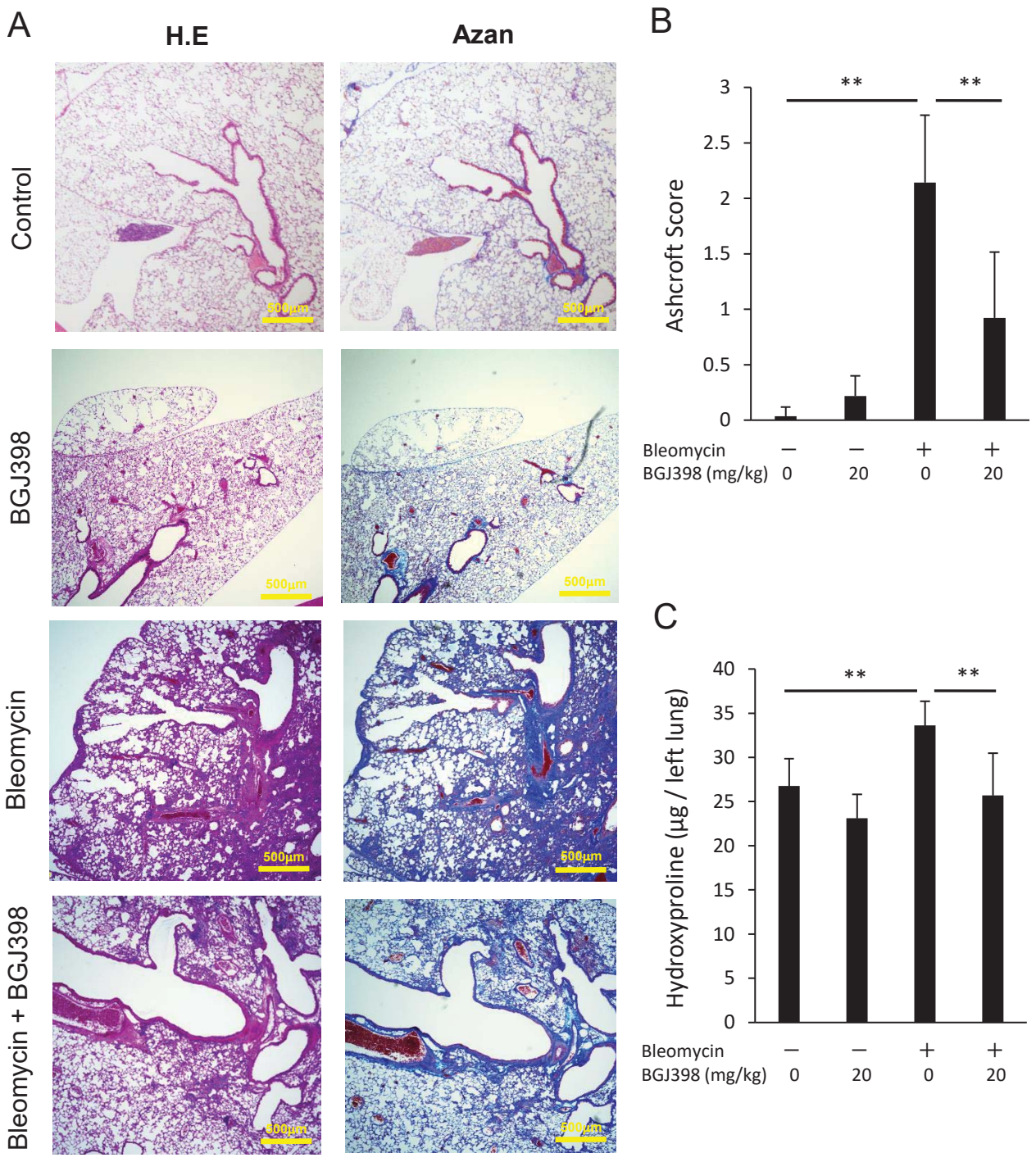

Figure 4

AJRCMB Articles in Press. Published April 27, 2020 as 10.1165/rcmb.2019-0090OC

A

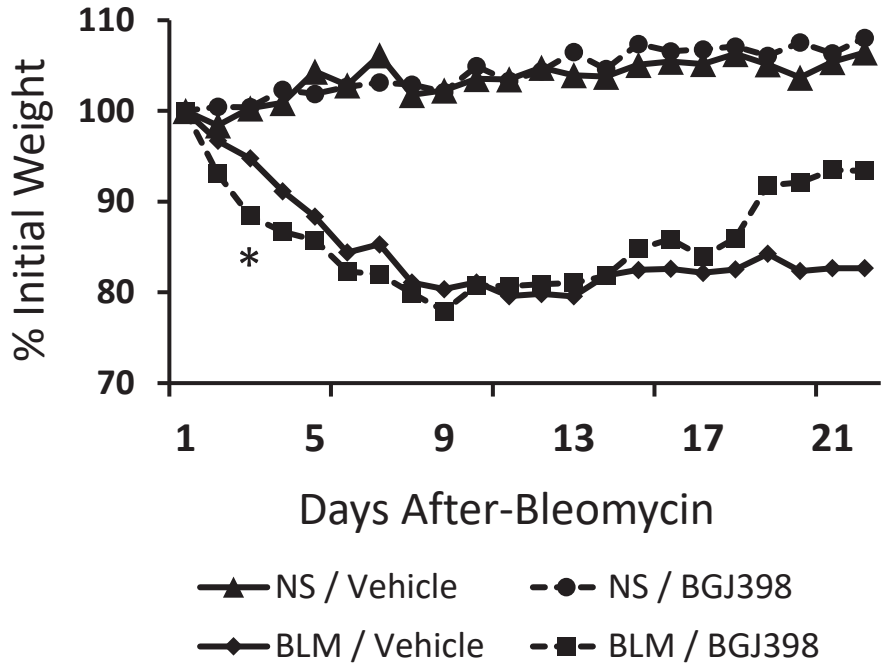

B

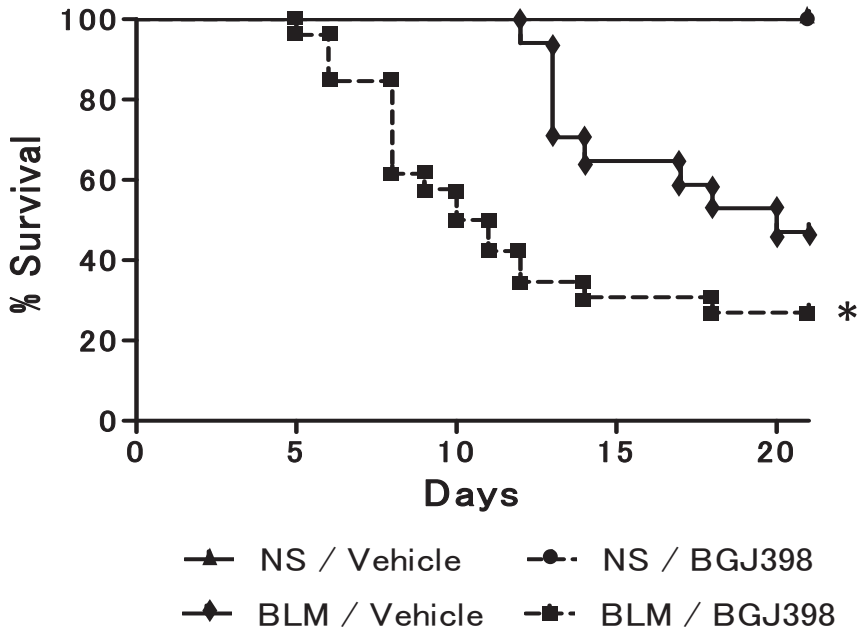

Figure 5

AJRCMB Articles in Press. Published April 27, 2020 as 10.1165/rcmb.2019-0090OC

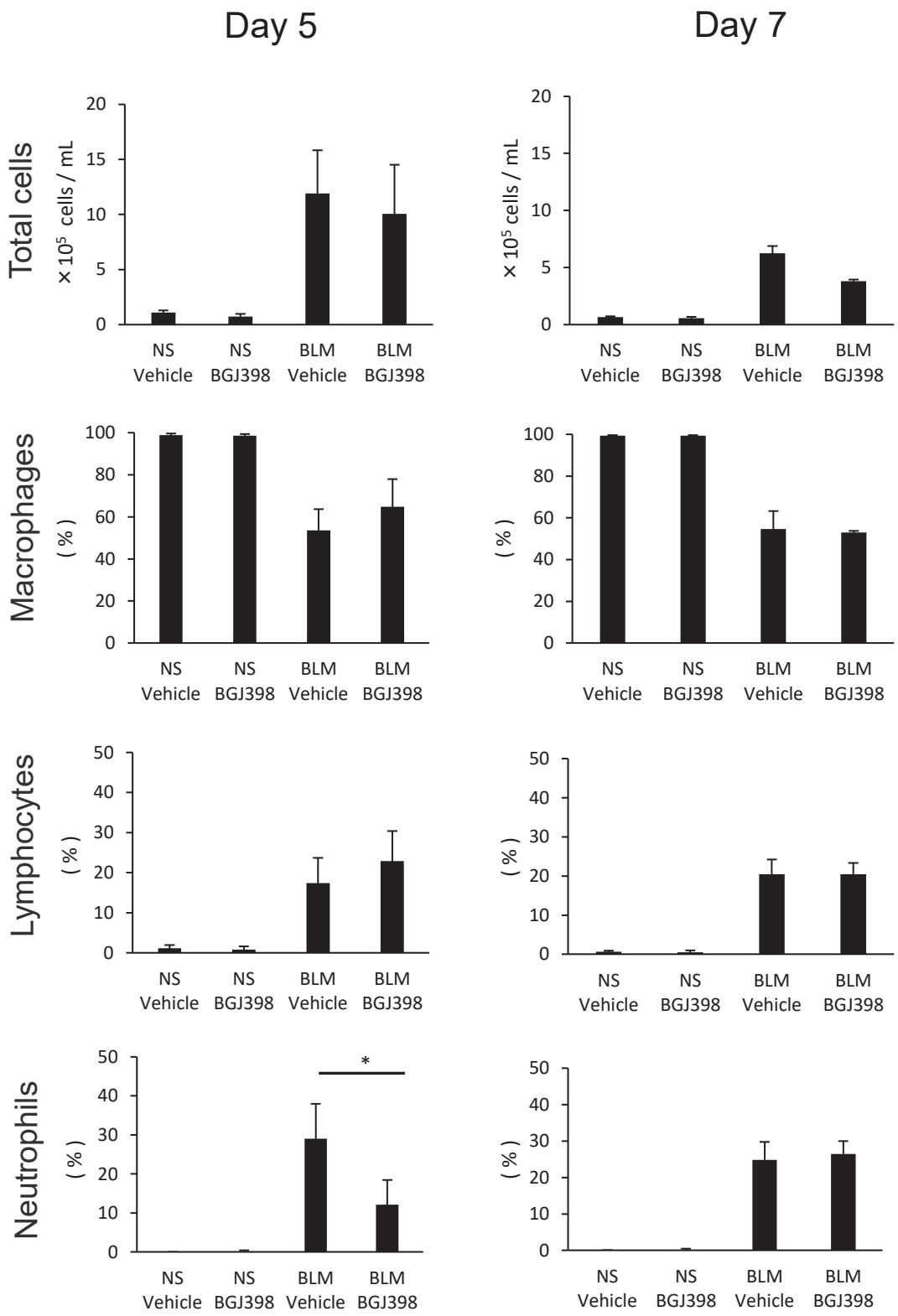

Figure 6

AJRCMB Articles in Press. Published April 27, 2020 as 10.1165/rcmb.2019-0090OC

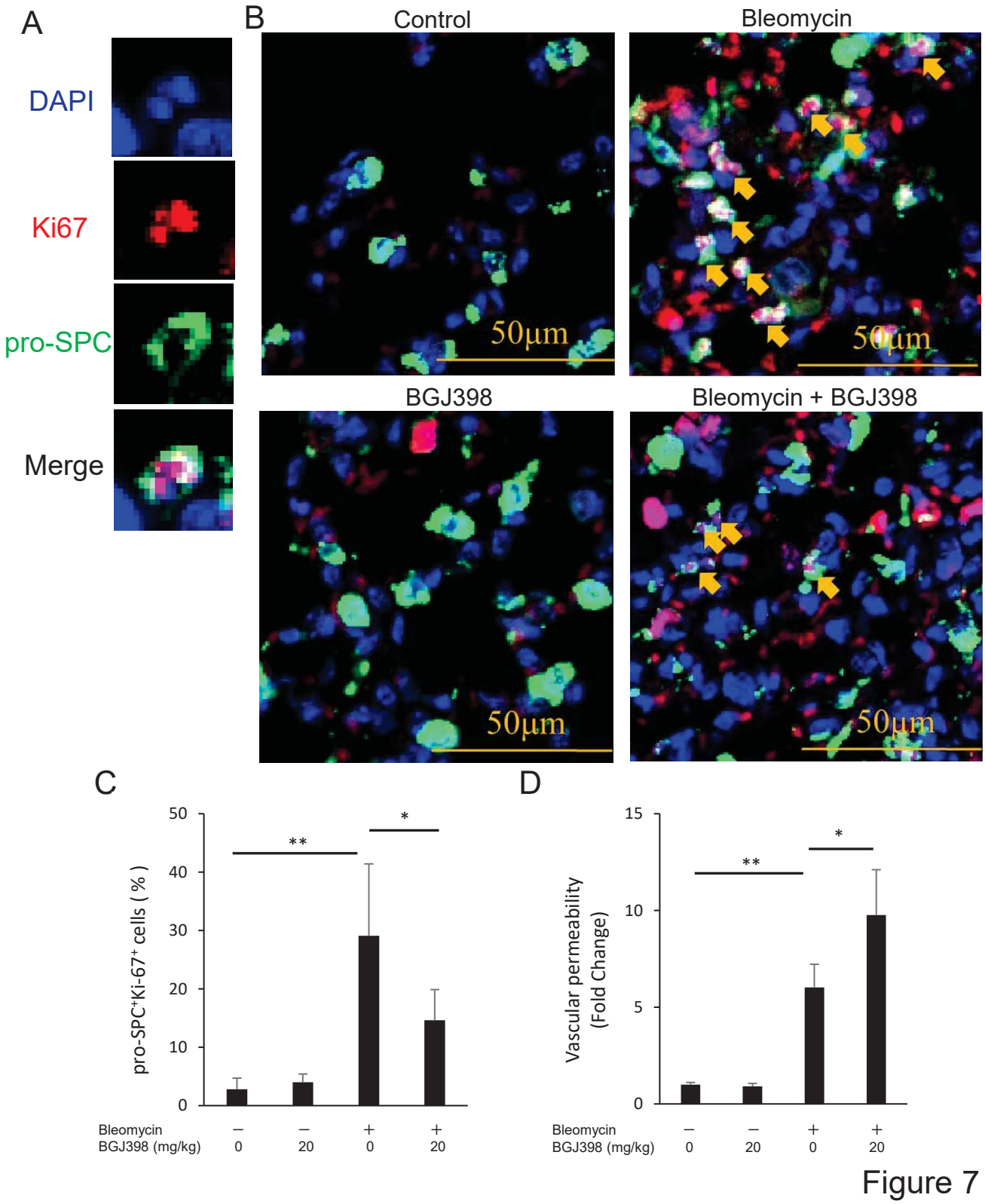

Figure 7

AJRCMB Articles in Press. Published April 27, 2020 as 10.1165/rcmb.2019-0090OC

Blockade of pan-fibroblast growth factor receptors mediates bidirectional effects in lung fibrosis

Shun Morizumi[1], Seidai Sato[1], Kazuya Koyama[1], Hiroyasu Okazaki[1], Yajuan Chen[1], Hisatsugu Goto[1], Kozo Kagawa[1], Hirohisa Ogawa[2], Haruka Nishimura[1], Hiroshi Kawano[1], Yuko Toyoda[1], Hisanori Uehara[3], Yasuhiko Nishioka[1]

[1]Department of Respiratory Medicine and Rheumatology, Graduate School of Biomedical Sciences, Tokushima University, Tokushima, Japan

[2]Department of Pathology and Laboratory Medicine, Graduate School of Biomedical Sciences, Tokushima University, Tokushima, Japan

[3]Division of Pathology, Tokushima University Hospital, Tokushima, Japan

AJRCMB Articles in Press. Published April 27, 2020 as 10.1165/rcmb.2019-0090OC

SUPPLEMENTAL DATA

Materials and Methods

BGJ398 was purchased from Chemietek (Indianapolis, IN, USA). Bleomycin (BLM) was purchased from Nippon Kayaku Co. (Tokyo, Japan). Recombinant FGF2 was purchased from PeproTech (Rocky Hill, NJ, USA). Recombinant Human TGF-beta 1 was purchased from R&D Systems, Inc. (Minneapolis, MN, USA). FGF Receptor 1 (D8E4) XP Rabbit mAb was purchased from Cell Signaling Technology (Danvers, MA, USA). FGF Receptor 2 (D4L2V) Rabbit mAb was purchased from Cell Signaling Technology (Danvers, MA, USA). Anti-FGFR3 antibody [EPR2304(3)] and Anti-FGFR4 antibody were purchased from Abcam (Cambridge, UK). FITC-conjugated anti-mouse CD326 (Ep-CAM) (BioLegend; San Diego, CA, USA), FGF Receptor 1 (D8E4) XP Rabbit mAb (PE Conjugate) (Cell Signaling Technology, Danvers, MA, USA), PE-conjugated rabbit anti-FGF receptor 2 Antibody (LSBio; Seattle, WA, USA), and anti-pro-surfactant Protein C antibody (Abcam; Cambridge, UK) were used. Monoclonal antibody to Ki-67 was purchased from Acris (Herford, Germany). Evans Blue dye was obtained from Sigma-Aldrich (St. Louis, MO, USA). Anti-cleaved caspase-3 antibody was purchased from Cell Signaling Technology (Danvers, MA, USA). Anti-alpha smooth muscle actin antibody was purchased from Abcam (Cambridge, UK). DNA Damage Detection Kit (γH2AX) was purchased from Dojindo (Kumamoto, Japan).

AJRCMB Articles in Press. Published April 27, 2020 as 10.1165/rcmb.2019-0090OC

Cell lines

The human lung fibroblast cell line, MRC-5, was purchased from DS PHARMA BIOMEDICAL (Osaka, Japan). The murine fibroblasts, B6 were primary cultured from lung tissue of C57BL/6 mice. Two murine epithelial cell lines, LA4 and MLE12 were purchased from the American Type Culture Collection, ATCC (Manassas, VA, USA). Cells were maintained in DMEM or RPMI medium (MRC-5 and B6; DMEM, LA4 and MLE12; RPMI) supplemented with 10% FBS, penicillin (100 U/ml), and streptomycin (50 μg/ml). All cells were cultured at 37°C in a humidified atmosphere of 5% CO_2 in air.

Isolation of primary murine alveolar epithelial cells

Lung tissues of C57BL/6 mice were excised and minced, and then treated with collagenase to obtain a single cell suspension. Subsequently, cells were stained with FITC-conjugated anti-Ep-CAM antibody, and the positive cells were used as alveolar epithelial cells for flow cytometry.

Proliferation assay

Human lung fibroblasts (8×10^3 cells/well), murine lung fibroblasts (8×10^3 cells/well), or murine lung epithelial cells (LA4; 4×10^3 cells/well) were seeded on a 96-well plate, and cultured with various concentration of FGFR inhibitor BGJ398 (10-1000 nM) in the presence of FGF2 (30 ng/ml) for 48 hours. One μCi/well of [^{3}H] thymidine deoxyribose (^{3}H-TdR) was

AJRCMB Articles in Press. Published April 27, 2020 as 10.1165/rcmb.2019-0090OC

pulsed for the final 24 hours and the incorporation of ^{3}H-TdR was measured using a liquid scintillation counter (E1).

Cell migration assay

Human or murine lung fibroblasts in DMEM containing 0.1% of FBS were plated to the upper chamber of an 8-μm-pore cell culture insert (BD Bioscience, San Jose, CA, USA) in the presence or absence of various concentrations of inhibitors. FGF2 (30 ng/mL) was added to the lower chamber. After 24-hour incubation, cells that had migrated to the bottom surface of the filter were stained with Diff-Quick (Baxter, Miami, FL) and counted (E2).

Immunoblot analysis

Cell extracts of murine fibroblast cells (B6) and alveolar epithelial cells (LA4, MLE12) were collected after culturing in DMEM (B6) or RPMI (LA4, MLE12) containing 10% FBS. Whole cell extracts and homogenized lung tissues were prepared with M-PER reagents (Thermo Fisher Scientific, Waltham, MA USA) containing phosphatase and protease inhibitor cocktails (Roche, Basel, Switzerland). Protein concentrations were measured using the Bradford method. The same amounts of total cell extract proteins were electrophoresed on 4-10% NuPAGE Bis-tris Mini Gels and transferred onto polyvinylidene difluoride membranes (Millipore, Billerica, MA) using the WSE-4040 HorizeBLOT 4M-R system (ATTO, Tokyo, Japan). The membrane was treated with the blocking agent Blocking One (Nacalai Tesque) for one hour and incubated at 4℃ overnight with the first antibodies. Following four-times washes, the membrane was

AJRCMB Articles in Press. Published April 27, 2020 as 10.1165/rcmb.2019-0090OC

incubated with horseradish peroxidase-conjugated secondary antibodies (1:2000 dilution, GE Healthcare, Fairfield, CT) in buffer at room temperature for one hour. The membrane was developed using Amersham ECL Western Blotting Detection Reagents (GE Healthcare, Fairfield, CT), and signals were detected using an enhanced chemiluminescence system (GE Healthcare, Fairfield, CT) (E3). The intensity of the bands was quantified using the public domain National Institutes of Health imaging program (W. Rasband, Reaserch Service Branch, National institutes of Health, Bethesda, MD, USA). The first antibodies used were as follows: anti-FGFR-1 antibody (1:1000 dilution, #9740S, Cell Signaling Technology, Danvers, MA), anti-FGFR-2 antibody (1:1000 dilution, #23328, Cell Signaling Technology, Danvers, MA), anti-FGFR-3 antibody (1:1000 dilution, ab133644, Abcam, Cambridge, UK), anti-FGFR-4 antibody (1:1000 dilution, ab119378, Abcam, Cambridge, UK), anti-proSPC antibody (1:1000 dilution, ab90716, Abcam, Cambridge, UK), and anti-β-actin antibody (1:200 dilution, sc-47778, Santa Cruz, Dallas, TX). Cleaved Caspase-3 (Asp175) Antibody (1:1000 dilution, #9661, Cell Signaling Technology, Danvers, MA). Anti-alpha smooth muscle actin antibody [1A4] (1:300, ab7817, Abcam, Cambridge, UK). DNA Damage Detection Kit - γH2AX (1:50, G265, Dojindo, Kumamoto, Japan). Densitometric analysis was performed using National Institutes of Health (NIH) Image J software.

Bleomycin-induced pulmonary fibrosis in mice

Seven to eight-week-old C57BL/6 mice were purchased from Charles River Japan (Yokohama,

AJRCMB Articles in Press. Published April 27, 2020 as 10.1165/rcmb.2019-0090OC

Japan). Mice were maintained in the animal facility of Tokushima University under specific pathogen-free conditions according to the guidelines of our university. The present study was approved by the Institutional Animal Care and Use Committee of Tokushima University (Permission Number: 14099). Mice received a single intra-tracheal instillation of 3 or 6 mg/kg bleomycin on day 0. BGJ398 was administered each day by gavage until day 21. Lung tissues analyzed on day 21 were used for the Ashcroft score (left lung) and hydroxyproline colorimetric assay (right lung) when 6 mg/kg bleomycin was used. Bilateral lung tissues were analyzed on day 21 for both assay when 3 mg/kg bleomycin was used.

Histopathology

Right lung tissues were harvested, fixed in 10% formalin, and embedded in paraffin. Three-micrometer-thick sections were stained with hematoxylin and eosin (H&E) or azan mallory. In the quantitative analysis, a numeric fibrotic scale was used (Ashcroft score) (E4). The mean score was considered to be the fibrotic score.

Bronchoalveolar lavage

BGJ398 was administered daily by gavage at 20 mg/kg until day 5 or 7 after an intra-tracheal instillation of 6 mg/kg NaCl or bleomycin on day 0. On day 5 or 7, bronchoalveolar lavage (BAL) was performed five times with saline (1 mL) using a soft cannula (E2). After counting the number of cells in the BAL fluid (BALF), cells were cytospun onto glass slides and stained with Diff-Quick (Baxter, Miami, FL, USA) for cell classification. Protein concentrations of

AJRCMB Articles in Press. Published April 27, 2020 as 10.1165/rcmb.2019-0090OC

supernatant of BALF were measured using the Bradford method.

Flow cytometric analysis

The minced lungs were digested, and harvested single-cell suspensions were stained with anti-Ep-CAM Ab (#118207, BioLegend), anti-FGFR-1 Ab (#12777, Cell Signaling Technology), and anti-FGFR-2 Ab (#LS-C214234, LSBio). The stained cells were analyzed by a FACScan flow cytometer as previously described (BD Biosciences-Pharmingen, San Diego, CA, USA) (E3).

Endothelial permeability

Evans Blue dye was utilized as a marker of the endothelial barrier function. C57BL/6 mice received an intranasal instillation of 3 mg/kg NaCl or bleomycin on day 0. After seven days, mice were sacrificed and analyzed. At three hours prior to termination, Evans Blue dye was injected via the tail vein, and the extravasation of dye into bronchial alveolar lavage fluid (BALF) was quantified by spectrophotometry (absorbance at 620 nm).

Immunofluorescence staining

After the paraffin-embedded lung sections were deparaffinized, the antigen was activated in an autoclave (120 ° C., 15 minutes) with Dako REAL™ Target Retrieval Solution (#S203130, Dako, Denmark). Lung sections were stained with primary antibodies (anti-pro-surfactant Protein C antibody (1:1000 dilution, ab90716, Abcam, Cambridge, UK) and Monoclonal

AJRCMB Articles in Press. Published April 27, 2020 as 10.1165/rcmb.2019-0090OC

antibody to Ki-67 (1:200 dilution, AM33074PU-N, Acris, Herford, Germany) at 4°C overnight and subsequently stained with fluorescence-conjugated secondary antibodies and 4', 6-diamidino-2-phenylindole at room temperature for 1 hour. Fluorescence images were captured with a confocal laser scanning microscope at 200x magnification (Nikon A1R resonant scanning confocal system, Tokyo, Japan). Double-positive cells for pro-SPC and Ki-67 were counted in 5 random fields (E3).

Quantitative real-time PCR

Total cellular RNA was isolated by acid guanidinium thiocyanate-phenol-chloroform extraction as described previously (E5) and reverse-transcribed into cDNA using the TaKaRa PCR Thermal Cycler Dice. Quantitative real-time PCR analysis was performed using the CFX96 real-time PCR system (Bio-Rad). Primers used for Figure E1 were previously described (E6).

In the experiments to examine the response to cytokines and growth factors of fibroblasts as well as the effects of BGJ398 on those (shown in Figure E10), Serum-starved lung fibroblast B6 cells were harvested in DMEM with 0.1% FBS and 1% penicillin-streptomycin. B6 cells were cultured in medium containing 30 ng/mL of FGF2 or 20 ng/ml of TGF-β1 together with 100 nM of BGJ398. Total cellular RNAs were extracted 12 hours after (for examining *Col1a1* expression and *Acta2* expression stimulated with FGF2, or *Col1a1* expression stimulated by TGF-β1) or 24 hours after (for examining *Acta 2* expression stimulated with TGF-β1). The

AJRCMB Articles in Press. Published April 27, 2020 as 10.1165/rcmb.2019-0090OC

sequences of primers used for Figure E10 were as follows:

Col1a1 forward, 5'-TCTGCGACAACGGCAAGGTG-3',

Col1a1 reverse, 5'-GACGCCGGTGGTTTCTTGGT-3',

Acta2 forward, 5'-GAGCGTGGCTATTCCTTCGT-3',

Acta2 reverse, 5'-GCCCATCAGGCAACTCGTAA-3',

Gapdh forward, 5'-GAAGGTGAAGGTCGGAGTC-3',

Gapdh reverse, 5'-GAAGATGGTGATGGGATTTC-3'.

Statistical Analysis

Significances of differences were analyzed by one-way ANOVA followed by Tukey's test or Student's *t*-test for unpaired samples. The survival curve was analyzed by log rank test. *P*-values of less than 0.05 were considered significant. Statistical analyses were performed using GraphPad Prism program Ver.5.01 (*GraphPad* Software Inc.)

AJRCMB Articles in Press. Published April 27, 2020 as 10.1165/rcmb.2019-0090OC

References

E1. Aono Y, Nishioka Y, Inayama M, Ugai M, Kishi J, Uehara H, Izumi K, Sone S. Imatinib as a novel antifibrotic agent in bleomycin-induced pulmonary fibrosis in mice. *Am J Respir Crit Care Med*. 2005;171:1279-1285.

E2. Aono Y, Kishi M, Yokota Y, Azuma M, Kinoshita K, Takezaki A, Sato S, Kawano H, Kishi J, Goto H, Uehara H, Izumi K, Nishioka Y. Role of platelet-derived growth factor/platelet-derived growth factor receptor axis in the trafficking of circulating fibrocytes in pulmonary fibrosis. *Am J Respir Cell Mol Biol* 2014;51:793-801.

E3. Sato S, Shinohara S, Hayashi S, Morizumi S, Abe S, Okazaki H, Chen Y, Goto H, Aono Y, Ogawa H, Koyama K, Nishimura H, Kawano H, Toyoda Y, Uehara H, Nishioka Y. Anti-fibrotic efficacy of nintedanib in pulmonary fibrosis via the inhibition of fibrocyte activity. *Respir Res.* 2017;18:172.

E4. Ashcroft T, Simpson JM, Timbrell V. Simple method of estimating severity of pulmonary fibrosis on a numerical scale. J Clin Pathol. 1988;41:467-470

E5. Chomczynski P, Sacchi N. The single-step method of RNA isolation by acid guanidinium thiocyanate-phenol-chloroform extraction: twenty-something years on. Nat Protoc 2006;1:581-585.

E6. Kurosu H, Choi M, Ogawa Y, et al. Tissue-specific expression of betaKlotho and fibroblast

AJRCMB Articles in Press. Published April 27, 2020 as 10.1165/rcmb.2019-0090OC

growth factor (FGF) receptor isoforms determines metabolic activity of FGF19 and FGF21. J Biol Chem 2007;282:26687-26695.

AJRCMB Articles in Press. Published April 27, 2020 as 10.1165/rcmb.2019-0090OC

Figure legends

Figure E1. The mRNA expression of receptors for fibroblast growth factors on murine lung fibroblasts and alveolar epithelial cells.

The relative levels of FGFR1 (A), FGFR2 (B), FGFR3 (C), and FGFR4 (D) in B6, MLE12, and LA4 cells were examined using RT-qPCR. Data are presented as means ± SDs.

Figure E2. Representative images for H.E and Azan-staining in NS/Vehicle group of Figure 4.

Three representative images for HE-stain, Azan-stain, and higher magnification images of HE-stain per NS/Vehicle mice-group is shown.

Figure E3. Representative images for H.E and Azan-staining in NS/BGJ398 group of Figure 4.

Three representative images for HE-stain, Azan-stain, and higher magnification images of HE-stain per NS/BGJ398 mice-group is shown.

Figure E4. Representative images for H.E and Azan-staining in BLM/Vehicle group of Figure 4.

Three representative images for HE-stain, Azan-stain, and higher magnification images of HE-stain per BLM/Vehicle mice-group is shown.

AJRCMB Articles in Press. Published April 27, 2020 as 10.1165/rcmb.2019-0090OC

Figure E5. Representative images for H.E and Azan-staining in BLM/BGJ398 group of Figure 4.

Three representative images for HE-stain, Azan-stain, and higher magnification images of HE-stain per BLM/BGJ398 mice-group is shown.

Figure E6. The late phase administration of BGJ398 reduces the lung fibrosis but increases mortality.

C57BL/6 mice received an intra-tracheal instillation of 6 mg/kg NaCl or bleomycin on day 0. BGJ398 was administered daily by gavage at 20 mg/kg from day 10 until day 21 (A). The Kaplan-Meier plot shows survival in each group (B) (n=10: NS / Vehicle, n=10: NS / BGJ398, n=19: BLM / Vehicle, n=20: BLM / BGJ398). The fibrotic changes in the lung were evaluated using a numeric fibrotic score. A histological examination of the right lung was performed using H&E staining (C) (n=8 in each group). Collagen content in the left lung lobe was measured using the hydroxyproline colorimetric assay (D) (n=10 in each group). Data were analyzed by one-way ANOVA and are presented as means ± SDs. For all graphs: * $p<0.05$, ** $p<0.01$ versus the value in the group treated with bleomycin only.

Figure E7. The administration of BGJ398 to mice with reduced dose of bleomycin attenuated the lung fibrosis.

C57BL/6 mice received an intra-tracheal instillation of 3 mg/kg NaCl or bleomycin on day 0.

AJRCMB Articles in Press. Published April 27, 2020 as 10.1165/rcmb.2019-0090OC

BGJ398 was administered daily by gavage at 20 mg/kg from day 0 until day 21. The Kaplan-Meier plot shows survival in each group (A) (n=5 NS / Vehicle, n=5: NS / BGJ398, n=15: BLM / Vehicle, n=15: BLM / BGJ398). The fibrotic changes in the lung were evaluated using a numeric fibrotic score. A histological examination of the bilateral lung was performed using H&E staining (B) (n=6 in each group). Collagen content in the left lung lobe was measured using the hydroxyproline colorimetric assay (C) (n=6 in each group). Data were analyzed by one-way ANOVA and are presented as means ± SDs. For all graphs: * $p<0.05$, ** $p<0.01$ versus the value in the group treated with bleomycin only.

Figure E8. The concentration of protein contained in BALF supernatant was increased in bleomycin-treated group, but not changed by BGJ398.

C57BL/6 mice received an intra-tracheal instillation of 6 mg/kg NaCl or bleomycin on day 0. BGJ398 was administered daily by gavage at 20 mg/kg until day 5 or 7. Protein concentrations of supernatant of BALF were measured using the Bradford method. Data were analyzed by one-way ANOVA and are presented as means ± SDs. For all graphs: ** $p<0.01$ versus the value in the group treated with bleomycin only.

Figure E9. BGJ398 increased the expression of cleaved caspase-3 in bleomycin-treated lung, but decreased the expression of α-SMA.

C57BL/6 mice received an intra-tracheal instillation of 3 mg/kg NaCl or bleomycin on day 0. BGJ398 was administered daily by gavage at 20 mg/kg from day 0 until day 21. The

AJRCMB Articles in Press. Published April 27, 2020 as 10.1165/rcmb.2019-0090OC

expression of pro-SPC, cleaved caspase-3, and α-SMA was examined by immunoblot analysis. The cell extracts of murine lungs harvested on day 7 were used for cleaved caspase-3 (A, C), and those harvested on day 21 were used for α-SMA (B, D). The relative expression of each band was calculated by densitometric analysis.

Figure E10. BGJ398 inhibited the *Col1a1* and *Acta2* expression of fibroblasts upregulated by FGF2 but not TGF-β1.

Murine primary fibroblasts stimulated by 30 ng/ml of FGF2 (A) or 20 ng/ml of TGF-β1 (B) were cultured with 100 nM of BGJ398. The mRNA expression of *Col1a1* and *Acta2* of fibroblasts were examined by quantitative PCR.

Figure E11. Administration of BGJ398 increases the DNA damage of alveolar epithelial cells in bleomycin-induced pulmonary fibrosis in mice.

C57BL/6 mice received an intra-tracheal instillation of 6 mg/kg NaCl or bleomycin on day 0. BGJ398 was administered daily by gavage at 20 mg/kg until day 5. The lung tissue in each group was harvested and analyzed on day 5. (A) Representative images of immunofluorescence staining in each group are shown. Arrows indicate double-positive cells for pro-SPC and γH2AX (scale bar = 50 μm). Paraffin-embedded lung sections were stained with anti-pro-SPC antibody (*green*) and anti-γH2AX (*red*). (B) Representative images of immunofluorescence staining at a high magnification in bleomycin-treated lungs are shown to confirm the double-positive cells. (C) pro-SPC^{+}γH2AX^{+} cells, defined as DNA damaged, or apoptosis type II

AJRCMB Articles in Press. Published April 27, 2020 as 10.1165/rcmb.2019-0090OC

alveolar epithelial cells, were counted in 5 random fields per section at x200 magnification using lung sections. The results are shown as the ratio of Ki-67 positive cells in the total pro-SPC positive cells. (D) pro-SPC^{+} cells, defined as type II alveolar epithelial cells, were counted in 5 random fields per section at x200 magnification using lung sections. Data were analyzed by one-way ANOVA and are presented as means ± SDs. For all graphs: ** $p<0.01$ versus the value in the group treated with bleomycin only.

Figure E12. Expanded blots from Figure 1A.

Figure E13. Expanded blots from Figure E9.

AJRCMB Articles in Press. Published April 27, 2020 as 10.1165/rcmb.2019-0090OC

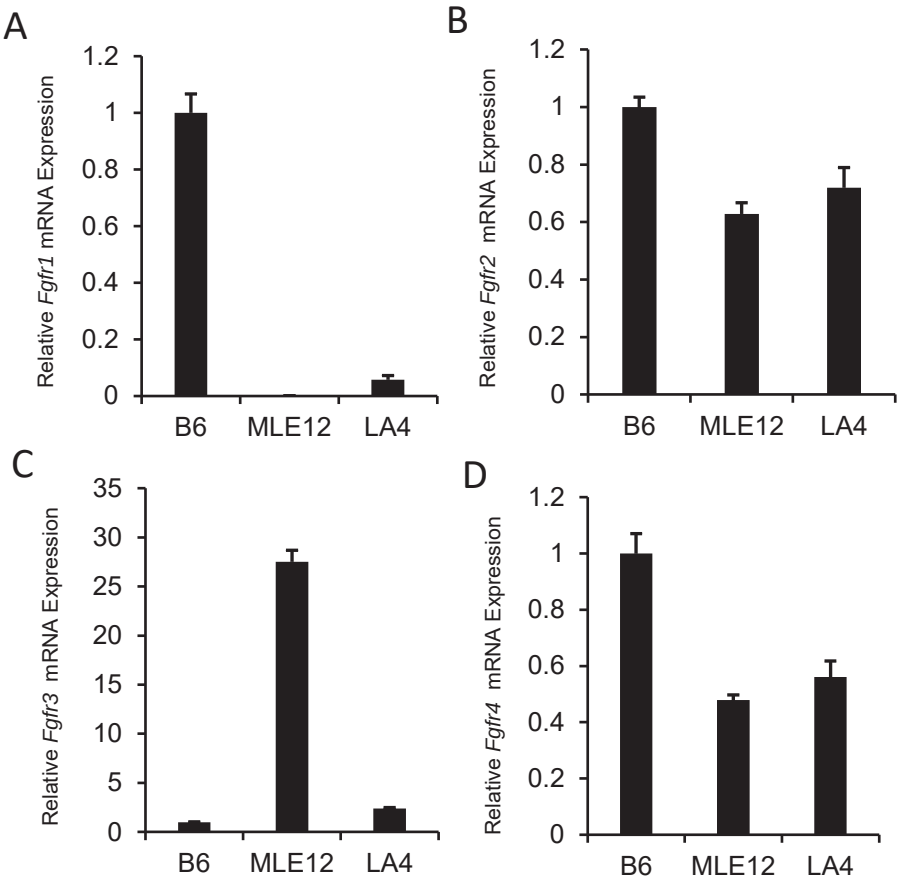

Figure E1

AJRCMB Articles in Press. Published April 27, 2020 as 10.1165/rcmb.2019-0090OC

NS / Vehicle

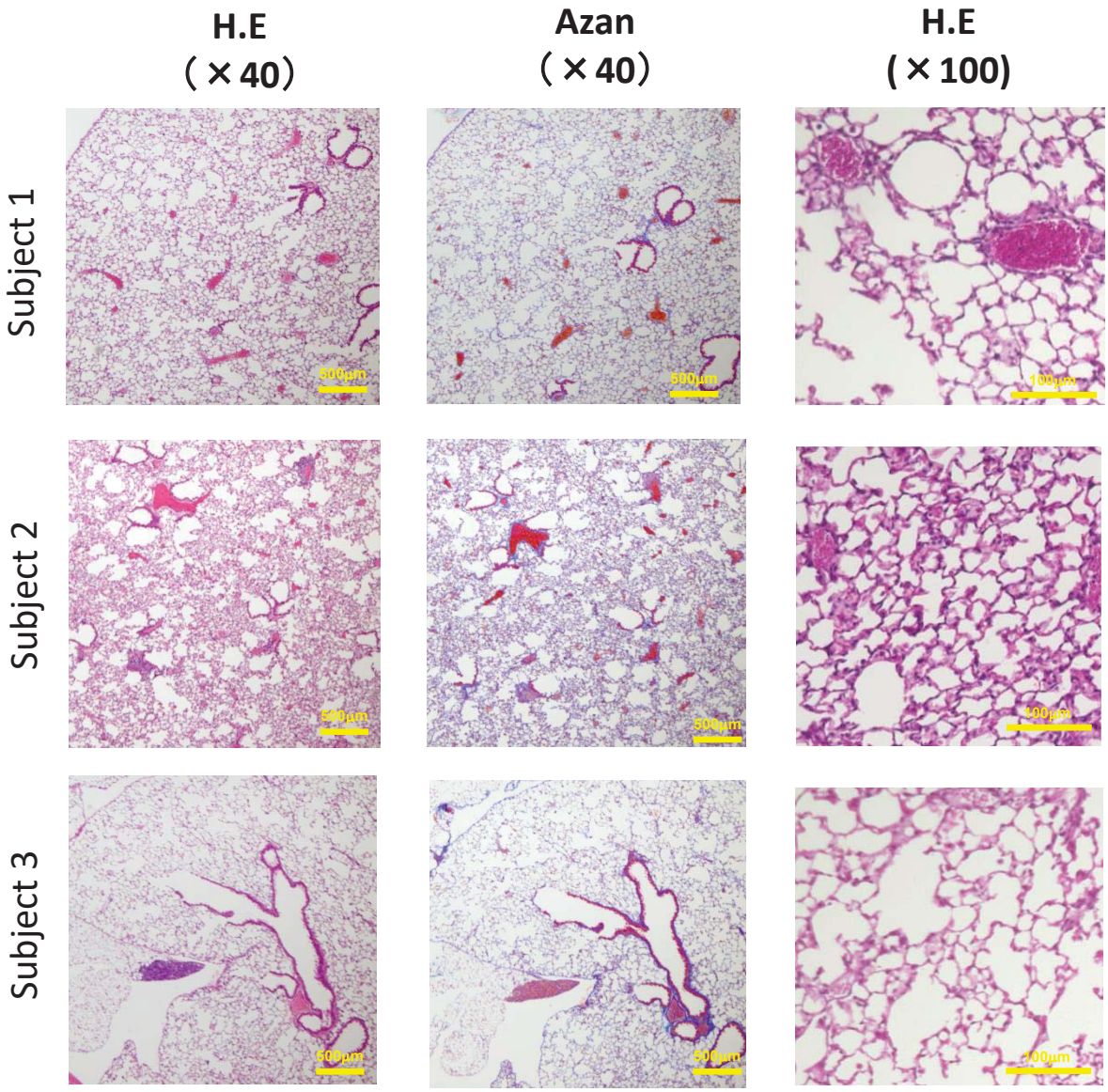

Figure E2

AJRCMB Articles in Press. Published April 27, 2020 as 10.1165/rcmb.2019-0090OC

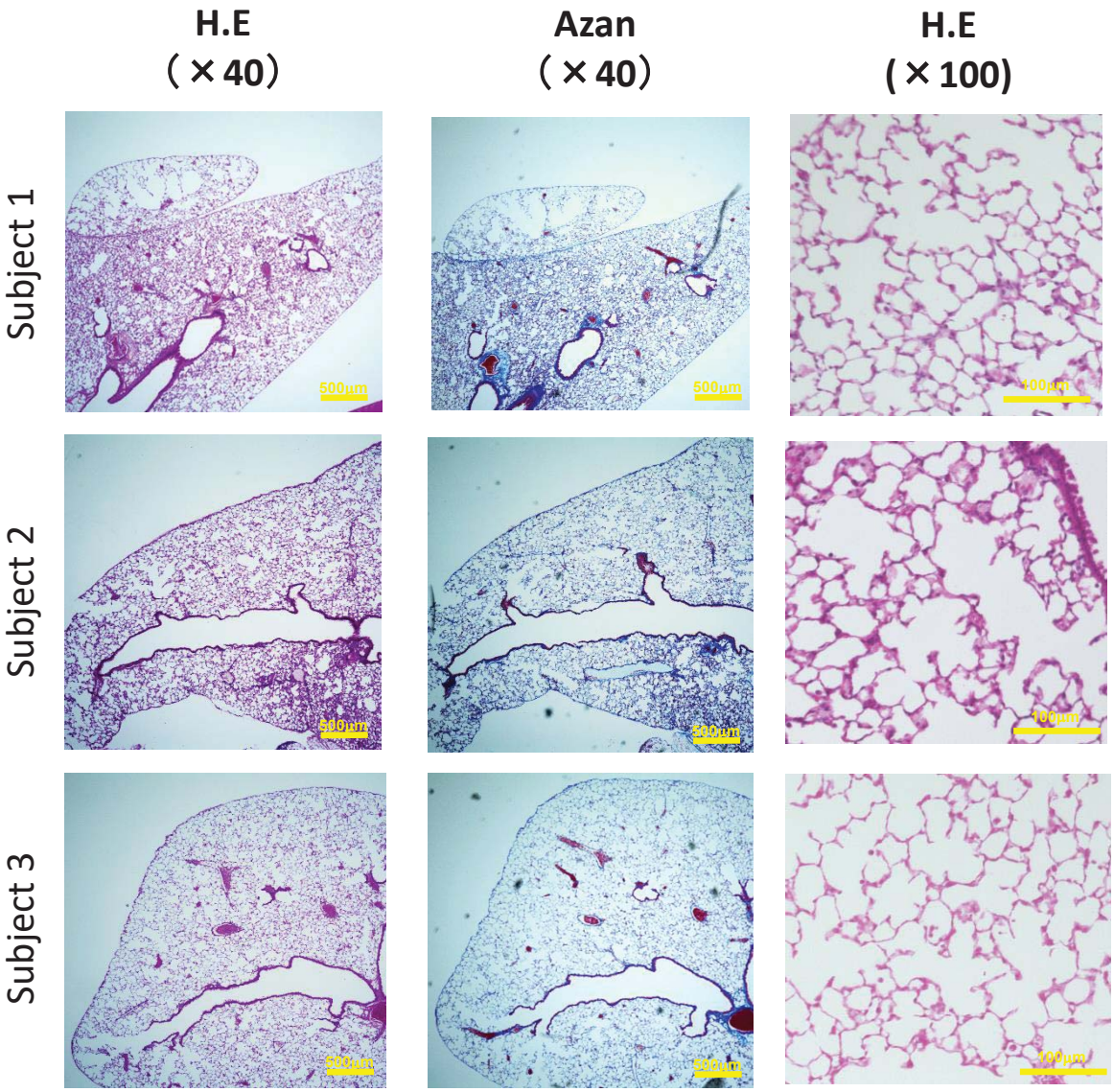

Figure E3

AJRCMB Articles in Press. Published April 27, 2020 as 10.1165/rcmb.2019-0090OC

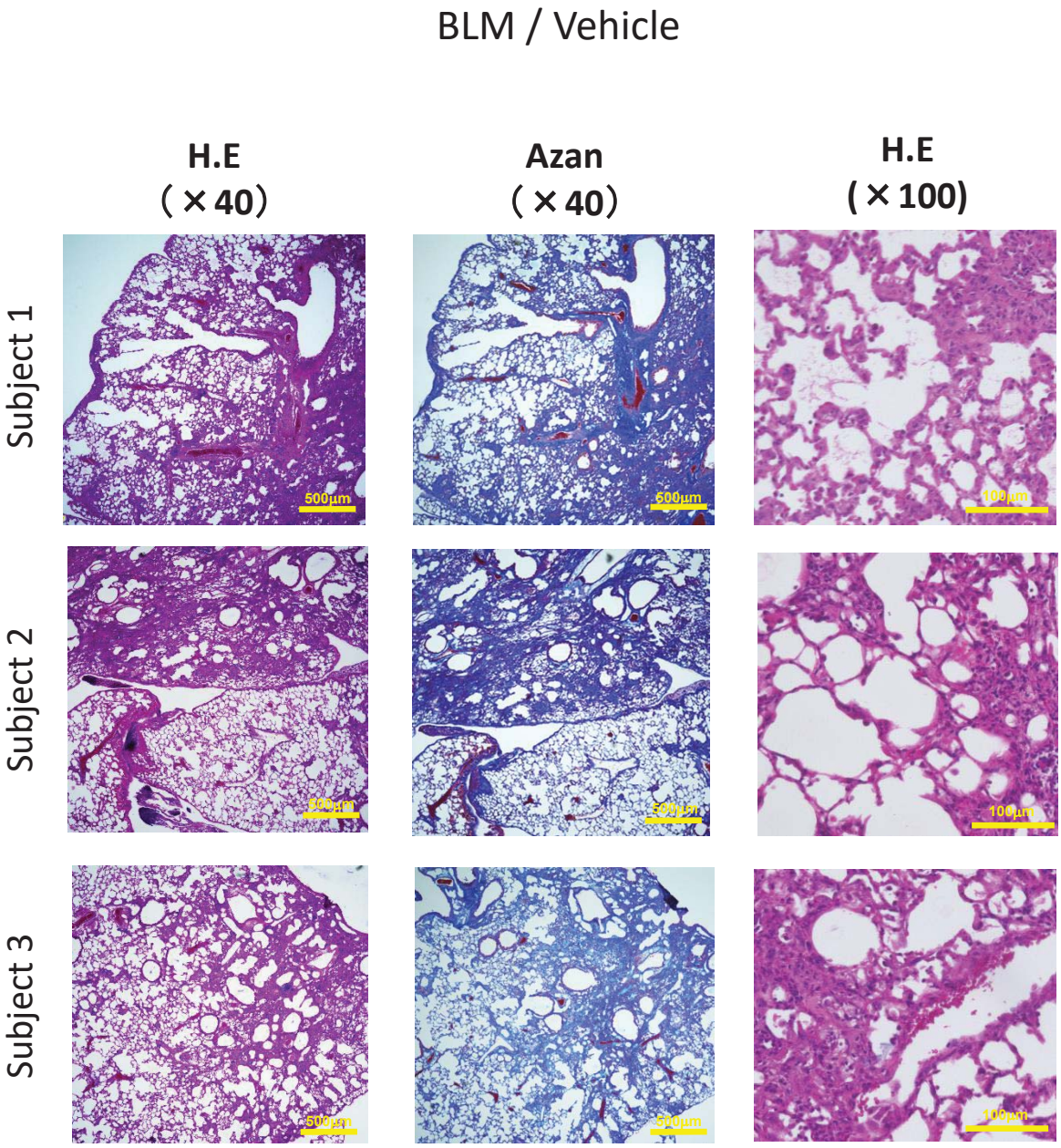

Figure E4

AJRCMB Articles in Press. Published April 27, 2020 as 10.1165/rcmb.2019-0090OC

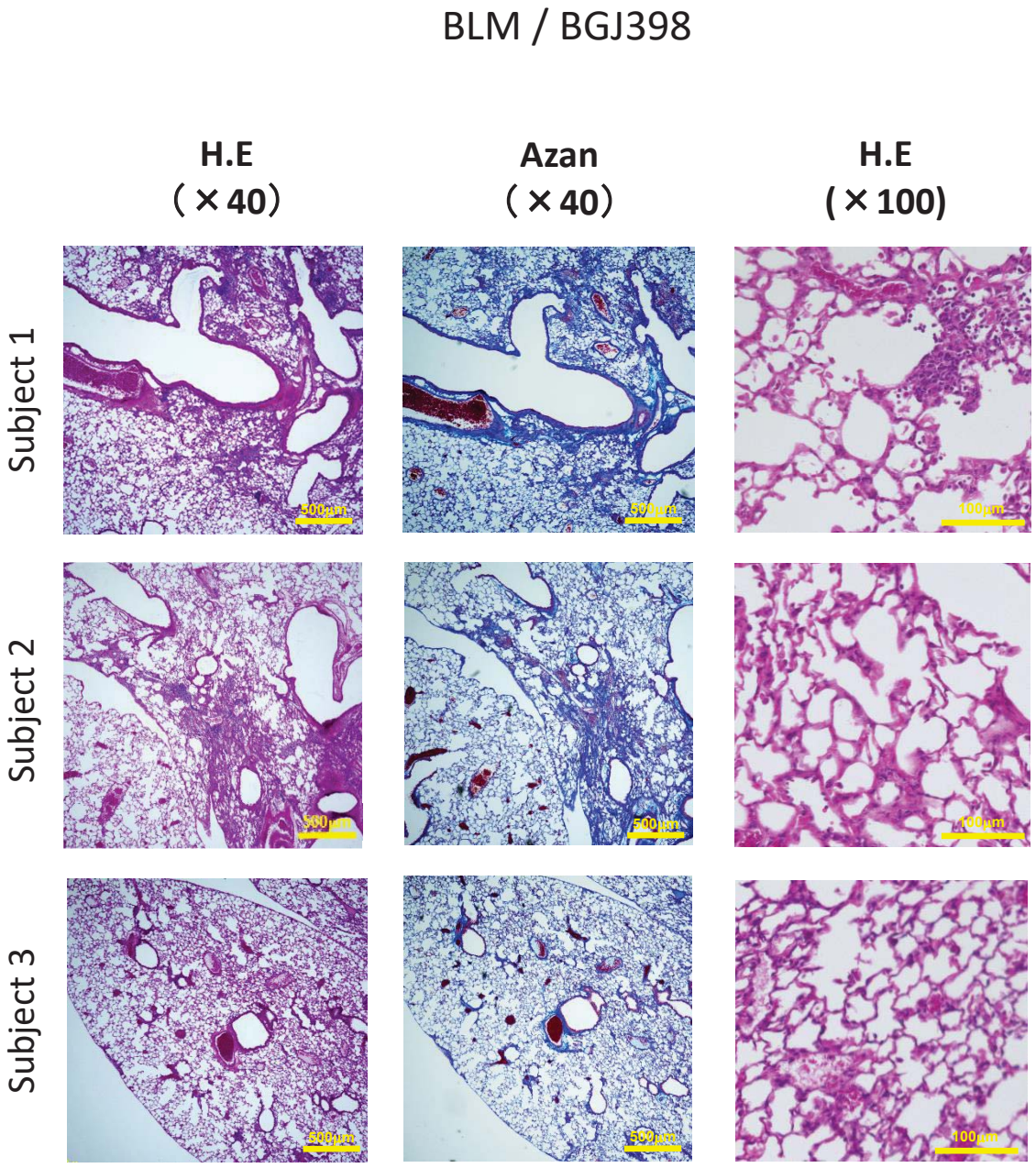

Figure E5

AJRCMB Articles in Press. Published April 27, 2020 as 10.1165/rcmb.2019-0090OC

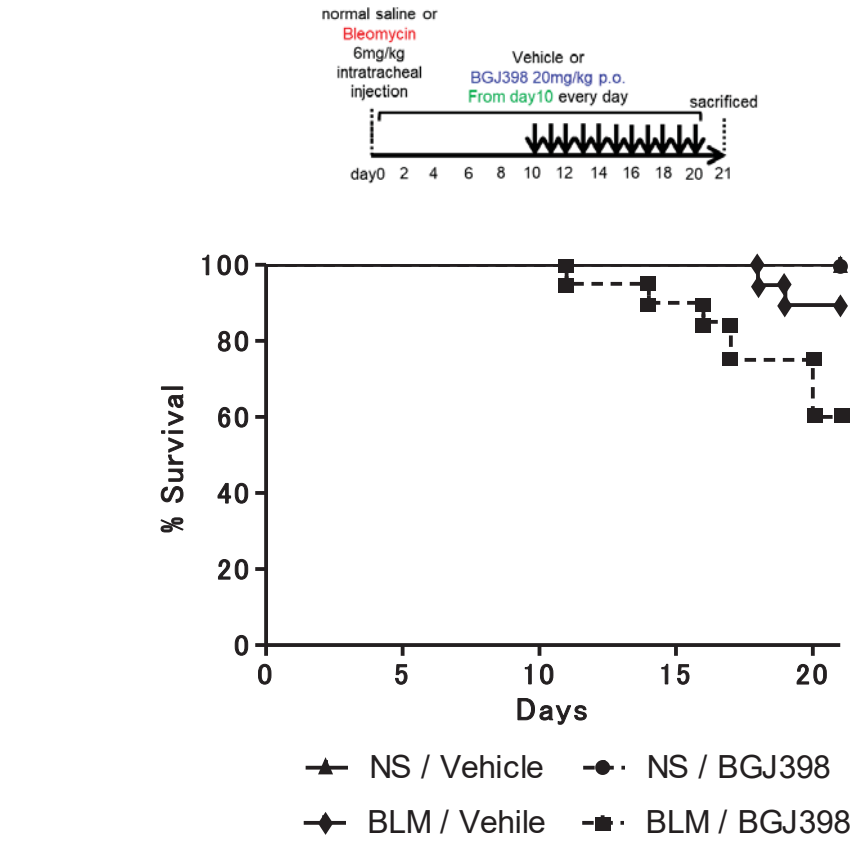

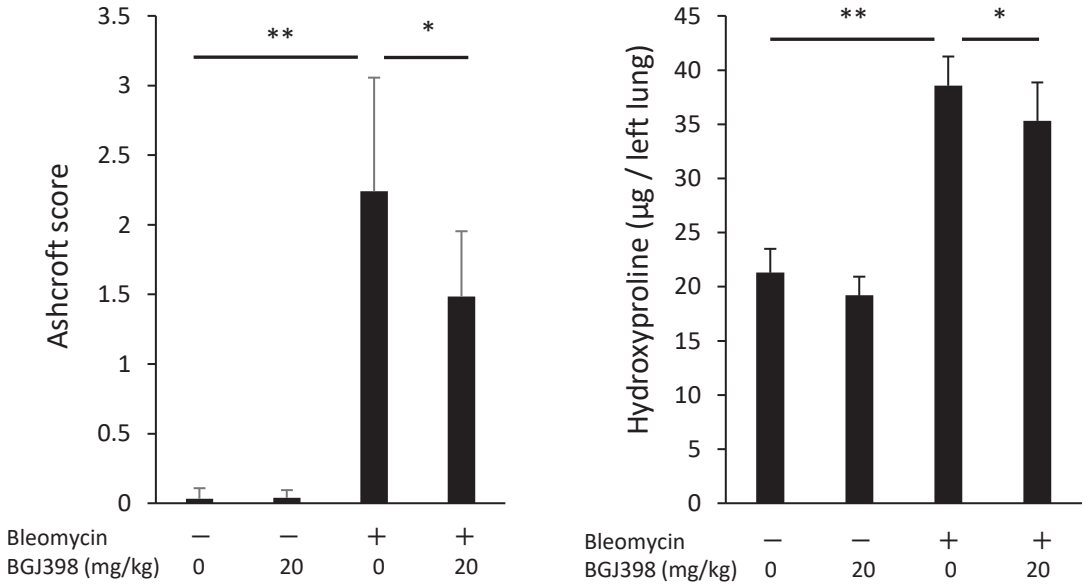

Figure E6

AJRCMB Articles in Press. Published April 27, 2020 as 10.1165/rcmb.2019-0090OC

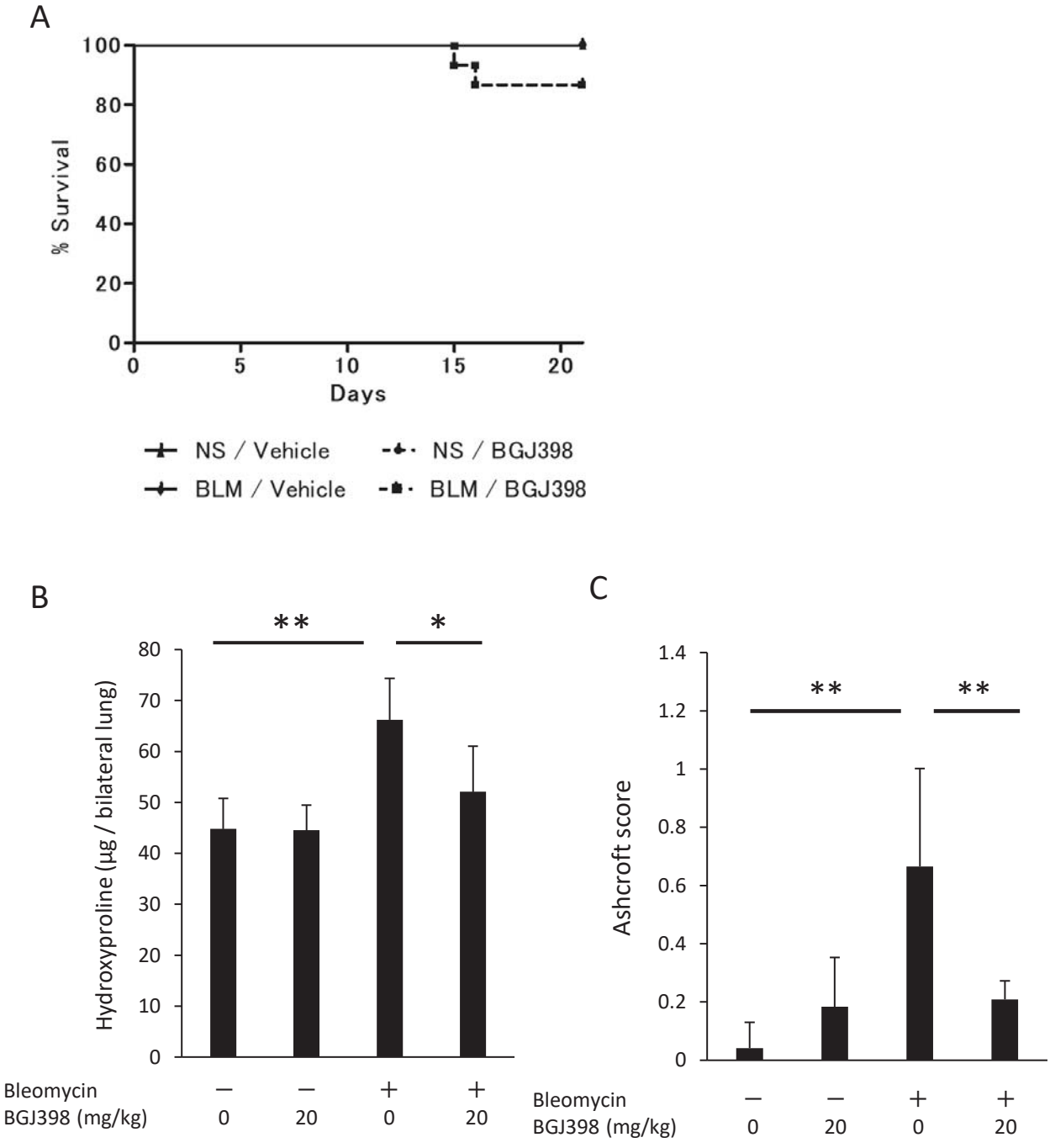

Figure E7

AJRCMB Articles in Press. Published April 27, 2020 as 10.1165/rcmb.2019-0090OC

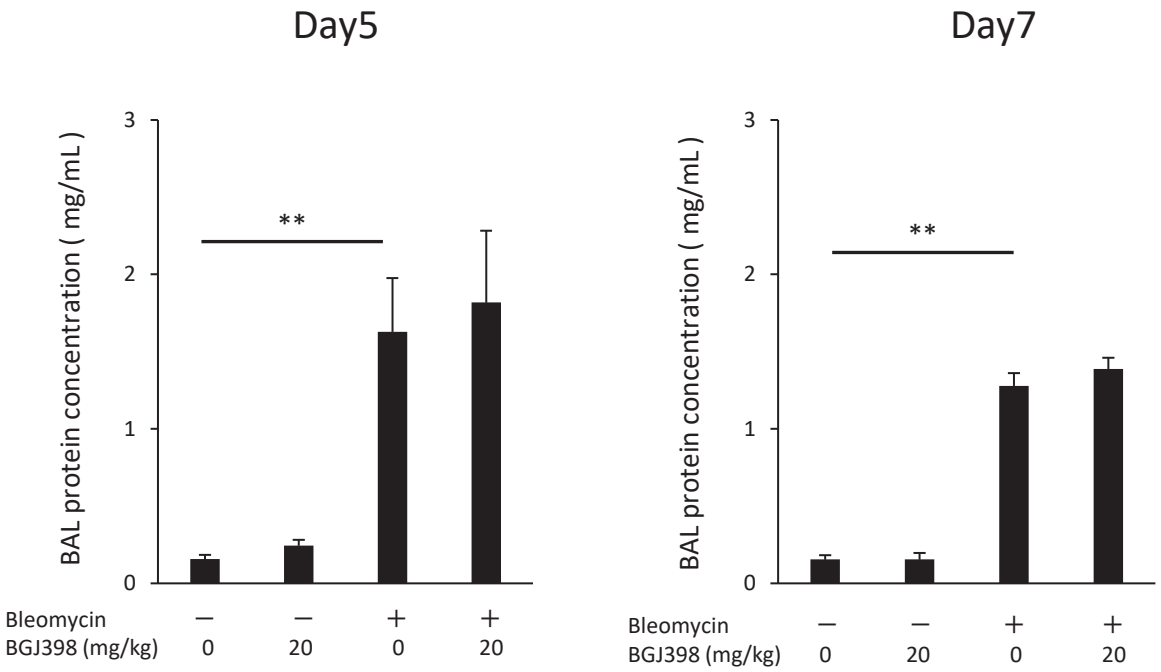

Figure E8

AJRCMB Articles in Press. Published April 27, 2020 as 10.1165/rcmb.2019-0090OC

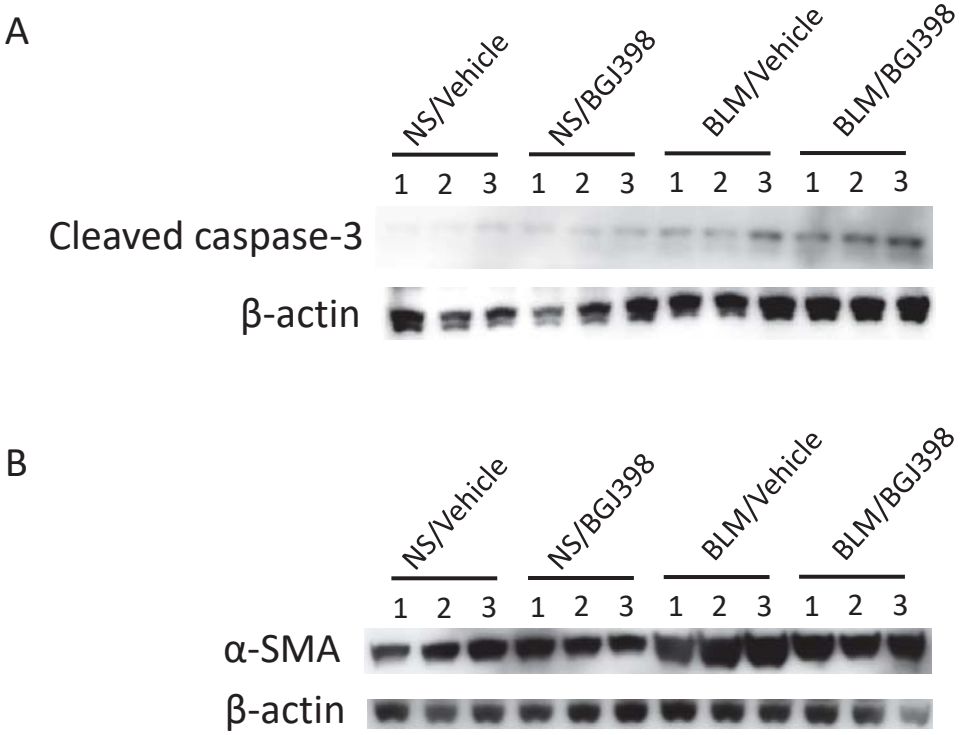

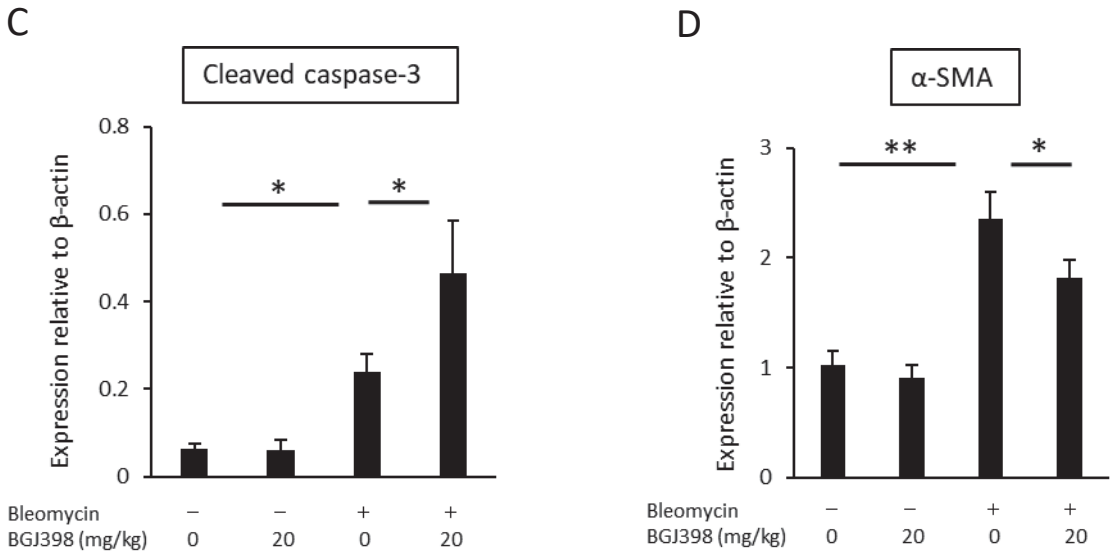

Figure E9

AJRCMB Articles in Press. Published April 27, 2020 as 10.1165/rcmb.2019-0090OC

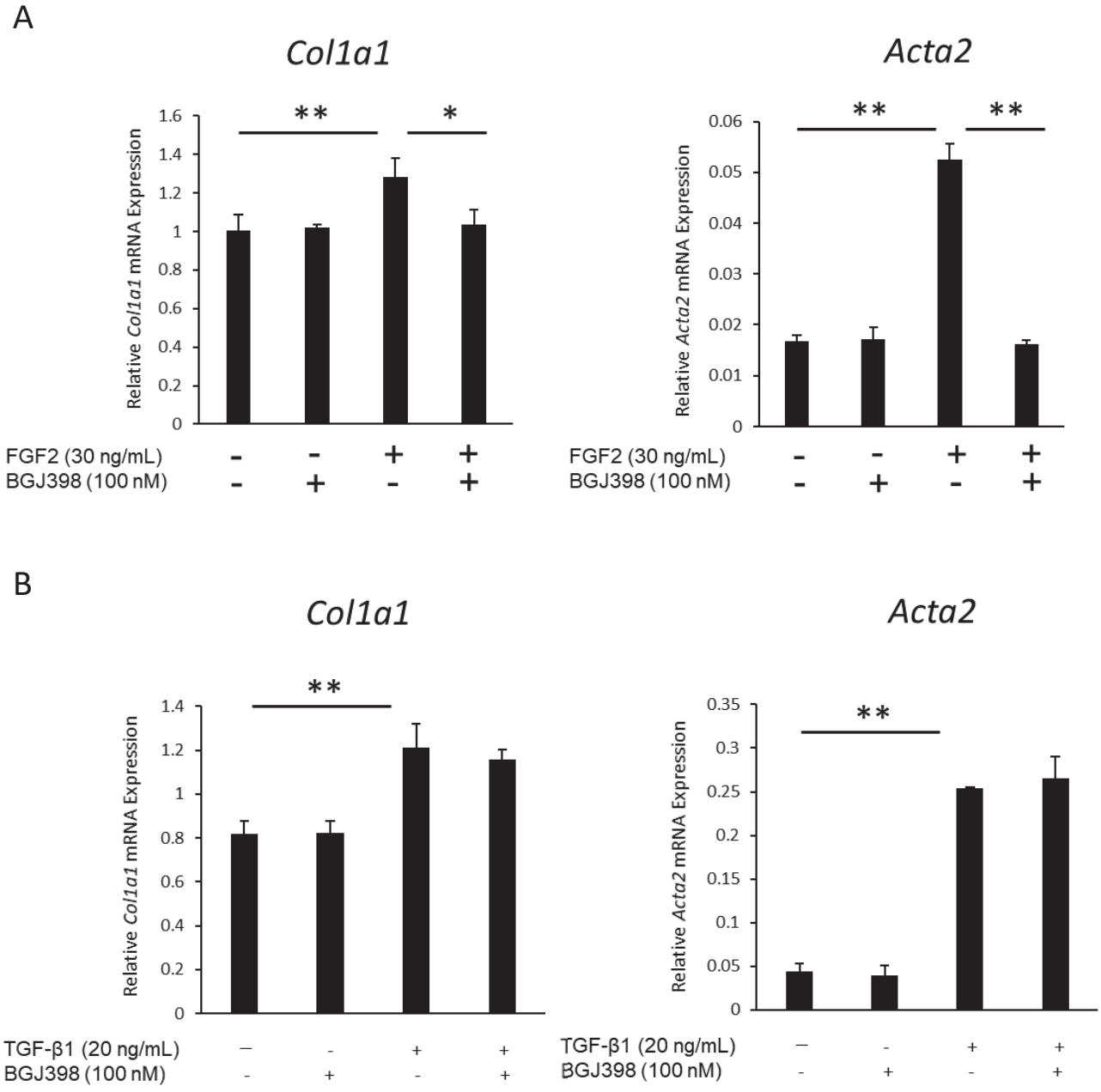

Figure E10

AJRCMB Articles in Press. Published April 27, 2020 as 10.1165/rcmb.2019-0090OC

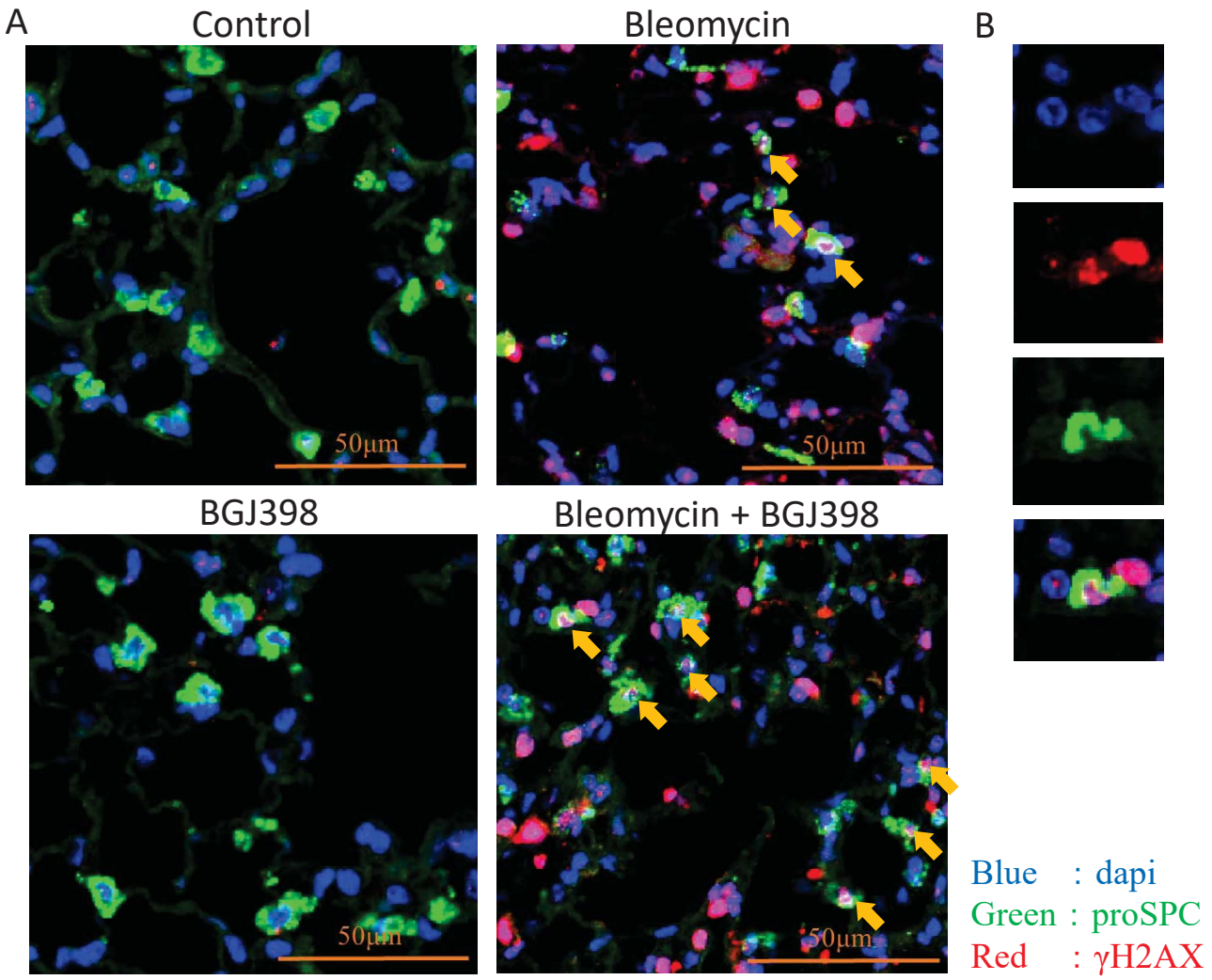

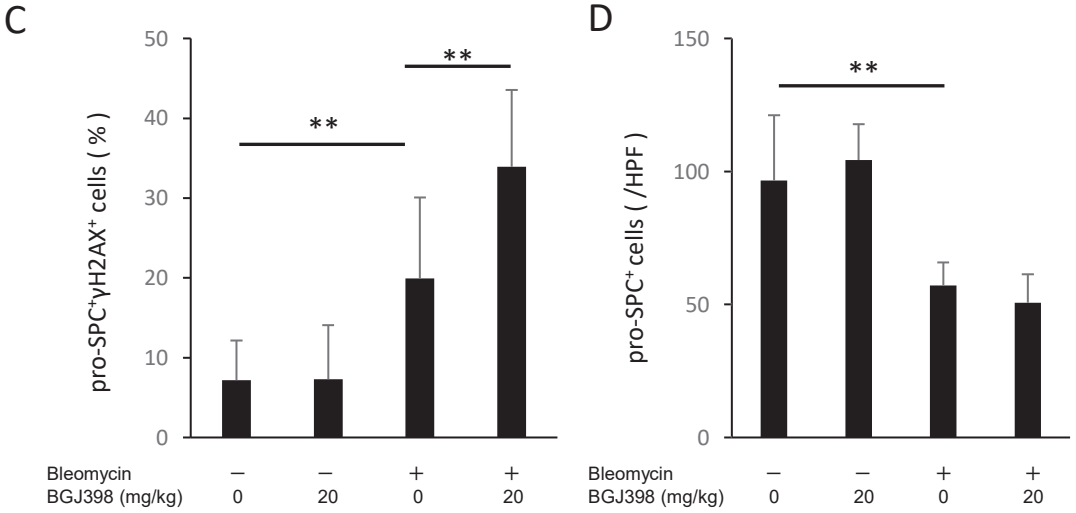

Figure E11

AJRCMB Articles in Press. Published April 27, 2020 as 10.1165/rcmb.2019-0090OC

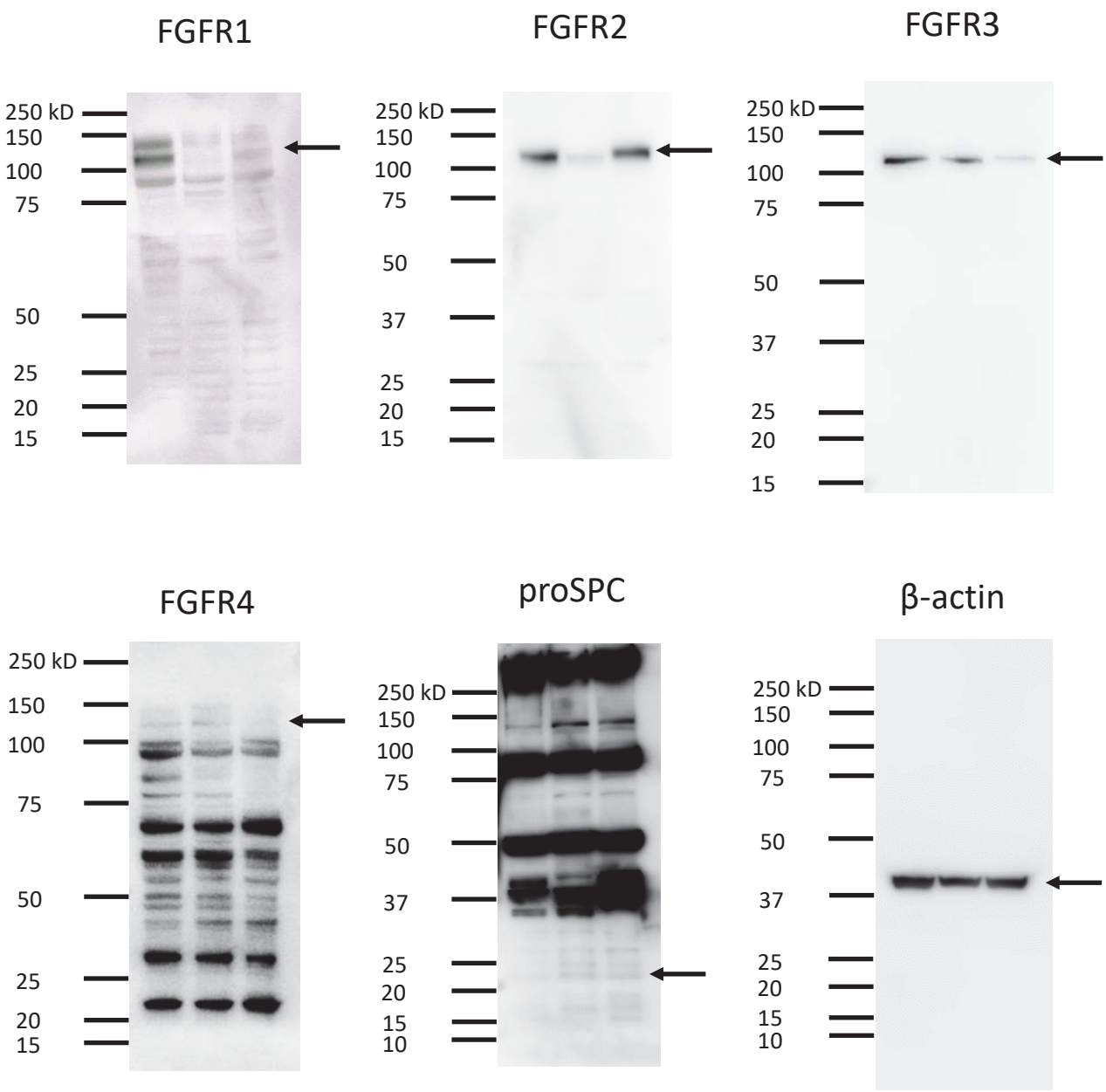

Figure E12

AJRCMB Articles in Press. Published April 27, 2020 as 10.1165/rcmb.2019-0090OC

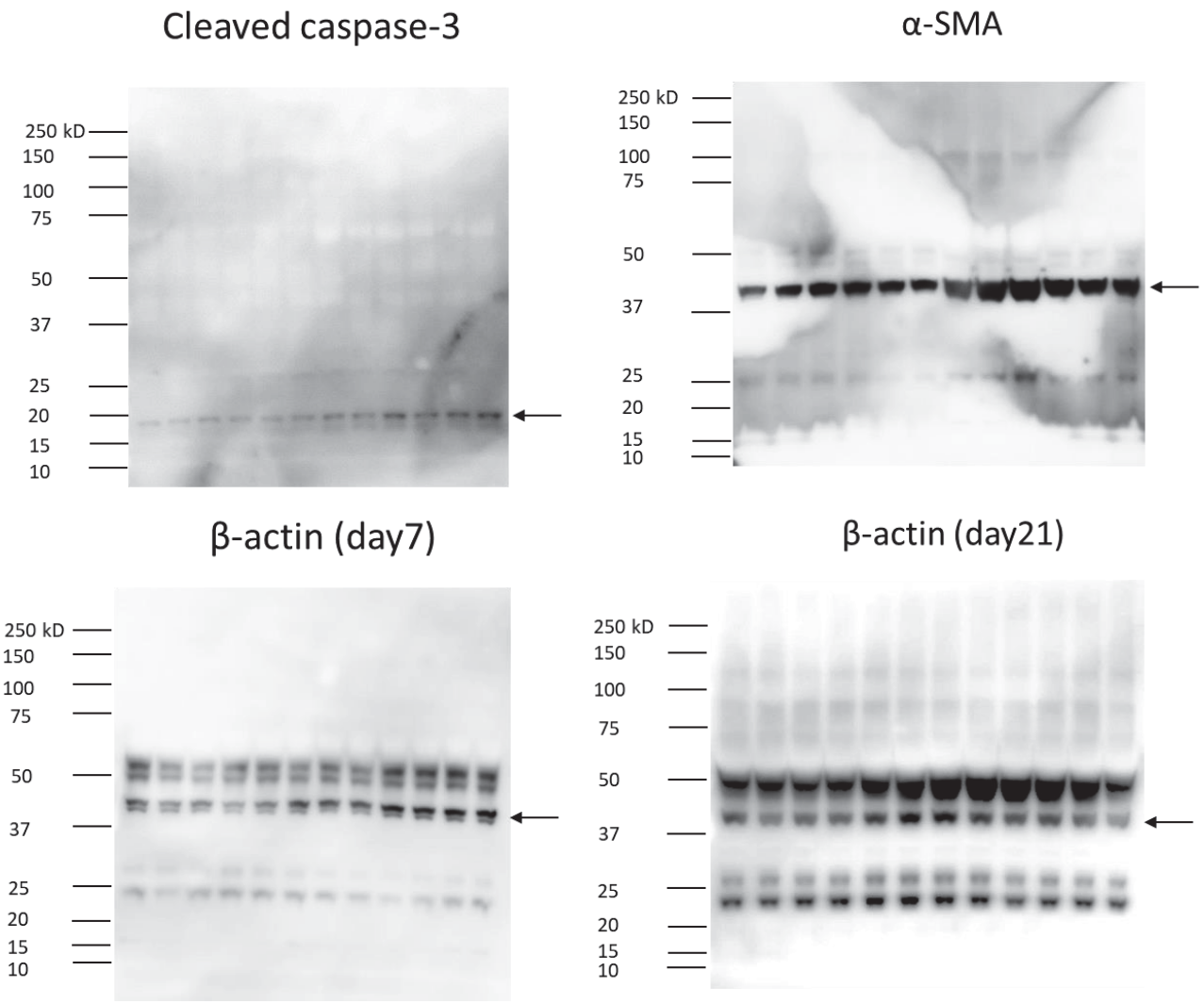

Figure E13

AJRCMB Articles in Press. Published April 27, 2020 as 10.1165/rcmb.2019-0090OC